Quantifying the Temporal and Spatial Response of Channel Steepness to Changes in Rift Basin Architecture

by

Scott M. Robinson

A Thesis Presented in Partial Fulfillment
of the Requirements for the Degree
Master of Science

Approved April 2014 by the
Graduate Supervisory Committee:

Arjun Heimsath, Co-Chair
Kelin Whipple, Co-Chair
Ramon Arrowsmith

ARIZONA STATE UNIVERSITY

May 2014

ABSTRACT

Quantifying the temporal and spatial evolution of active continental rifts contributes to our understanding of fault system evolution and seismic hazards. Rift systems also preserve robust paleoenvironmental records and are often characterized by strong climatic gradients that can be used to examine feedbacks between climate and tectonics. In this thesis, I quantify the spatial and temporal history of rift flank uplift by analyzing bedrock river channel profiles along footwall escarpments in the Malawi segment of the East Africa Rift. This work addresses questions that are widely applicable to continental rift settings: (1) Is rift-flank uplift sufficiently described by theoretical elliptical along-fault displacement patterns? (2) Do orographic climate patterns induced by rift topography affect rift-flank uplift or morphology? (3) How do uplift patterns along rift flanks vary over geologic timescales?

In Malawi, 100-km-long border faults of alternating polarity bound half-graben sedimentary basins containing up to 4km of basin fill and water depths up to 700m. Orographically driven precipitation produces climatic gradients along footwall escarpments resulting in mean annual rainfall that varies spatially from 800 to 2500 mm. Temporal oscillations in climate have also resulted in lake lowstands 500 m below the modern shoreline. I examine bedrock river profiles crossing the Livingstone and Usisya Border Faults in northern Malawi using the channel steepness index (Ksn) to assess importance of these conditions on rift flank evolution. River profiles reveal a consistent transient pattern that likely preserves a temporal record of slip and erosion along the entire border fault system. These profiles and other topographic observations, along with known modern and paleoenvironmental conditions, can be used to interpret a complete

history of rift flank development from the onset of rifting to present. I interpret the morphology of the upland landscape to preserve the onset of extensional faulting across a relict erosion surface. The linkages of individual faults and acceleration of slip during the development of a continuous border fault is suggested by an analysis of knickpoint elevations and Ksn. Finally, these results suggest that the modern observed climate gradient only began to significantly affect denudation patterns once a high relief rift flank was established.

TABLE OF CONTENTS

Page

LIST OF TABLES

Table Page

LIST OF FIGURES

Figure Page

CHAPTER 1

INTRODUCTION

Much attention involving a number of sub-disciplines within the earth sciences has been devoted to understanding the evolution of continental rift settings, yet the evolution of continental rift systems is still poorly understood. This knowledge gap is a function of the relatively low abundance of active continental rifts and the geographical location of existing active systems. Most identified rift systems are either inactive, for reasons that are poorly understood, or have advanced to the stage of oceanic rifting. Additionally, active systems are uncommon and often located in regions that present logistical challenges to field-based study. Despite these logistical challenges, these plate margins and intraplate extensional systems present tectonic hazards to large resource-limited populations.

A comprehensive understanding of rift basin evolution can aid in assessing active tectonic settings across different types of rift systems especially in the East Africa Rift System (EARS) (Figure 1). Despite this, we still no little about the temporal and spatial characteristics of major fault systems in rift settings, and what we do know is relies heavily on seismic reflection studies within sedimentary basins (Flannery et al., 1990; Contreras et al., 2000; Mortimer et al., 2007; Lyons et al., 2011). A better understanding of sub-aerial portions of this landscape is needed to develop a more in-depth model of crustal deformation in rift environments.

The structure of continental rifts also enables testing of integrated landscape evolution models. Appropriate field laboratories, where watershed/tectonic evolution can be directly coupled to a sedimentary basin that captures and faithfully records the history

of landscape evolution are rarely available (e.g., GeoPrisms, 2010; NRC, 2010a). Rift systems often create closed depositional systems, containing large lakes that preserve high-fidelity paleoenvironmental records that can be accessed via deep drilling and seismic analysis. These records are heavily influenced by climatic, tectonic, and autocyclic heterogeneities within the watershed and therefore are limited in what they can say about environmental conditions through time. An understanding of how upland systems evolve is essential if we hope to develop a better link between landscape evolution and sedimentary basins in order to best describe their interconnectivity and any feedbacks that might exist between them.

Reconstructing the history of upland landscapes is challenging because erosion reshapes the landscape. Our ability to detect subtle variations in topography that may reflect changing environmental conditions is subject to the resolution of topographic data available. Interpretations are also difficult within a landscape shaped by stochastic processes such as mass wasting events. High-relief, crystalline bedrock landscapes are well suited for interpreting erosional histories due to their relatively slow response time and high signal to noise ratio. Specifically, bedrock channel morphology can preserve a record of upland erosion over million year timescales and can be used to interpret spatial and temporal variation in various drivers of channel incision such as climate and tectonics (Whipple et al., 1999; Whipple, 2004; Dibiase et al., 2010).

Uplifted footwall blocks along major fault systems create continuous bedrock escarpments that define the trace of the EARS and present a unique opportunity to interpret the evolution of this rift-system via the upland topography. Because of similarities in observed structure across continental rift systems, analysis of a

representative rift environment can provide valuable insight transferable to other active rift systems. The Malawi Rift located near the southern end of the Western Branch of the EARS is considered by many to be an archetypal example of early stage continental rifting (Chorowicz, 2005). The two largest and most well developed fault systems in this section of the EARS, the Livingstone Border Fault System (LBFS) and Usisya Border Fault System (UBFS) respectively, define dramatic basins where bedrock escarpments abut Lake Malawi (figure 1). Seismic studies (Rosendahl et al., 1984; Ebinger et al., 1987; Mortimer et al., 2007; Lyons et al., 2011), scientific drill core analysis (Scholz et al., 2007; Cohen et al., 2007; Brown et al., 2007) and modern climate observations (Bookhagen et al., in review) provide detailed temporal and spatial context regarding basin structure and paleoenvironmental conditions that could be geomorphically significant. Specifically, seismic reflection data suggest that cumulative displacement along these fault systems loosely follows theoretical along-strike distributions and Scientific drill cores and modern climate observations have documented significant temporal and spatial variability in rainfall.

These observations, which will be discussed in more detail in the next section, inspire a suite of questions relating to the evolution of rift flanks: (1) Is rift-flank uplift well described by theoretical elliptical along fault displacement patterns? (2) Do orographic climate patterns induced by rift topography affect rift-flank uplift or morphology? (3) How do uplift patterns along rift flanks vary over geologic timescales? These questions can be addressed by utilizing along-strike topographic analysis and extracting temporal information from bedrock channels draining the escarpment and crossing the LBFS and UBFS traces. This information will provide valuable insight on

uplift patterns for neotectonic studies and the dynamics of upland denudation to aid in advancing geomorphic models.

CHAPTER 2

STUDY AREA

Geologic and Tectonic Setting

The East Africa Rift System (EARS) is separated into an eastern and western branch that together stretch from the Red Sea to South Africa (Figure 1). The physiographic manifestation of the rift is a long narrow series of valleys resulting from of crustal thinning. The narrowest and most well-defined basins occur over portions of the rift where deformation is concentrated on long 50-100km long border faults likely resulting from linkage of smaller scales faults that develop during the onset of extension (Cartwright et al., 1995). These border faults are typical of the western branch of the EAR which is dominated by asymmetric half grabens of alternating polarity linked together by complex accommodation zones (Rosendahl et al, 1992; Chorowicz, 2005). Rifting initiated in the younger western branch ~13 Ma and ~30 Ma in the eastern branch's Afar region of Ethiopia (Chorowicz, 2005). For this reason and because of structural similarities with other active and ancient rift systems, the western branch of the EAR is commonly studied as an early example of passive margin evolution.

The ~600km long Malawi Rift located at the southern terminus of the EARS is a continuation of the western branch (Figure 1). Similar to the rest of the western branch, the Malawi portion of the rift is characterized by active half-graben structures of alternating polarity. A southward decrease in initiation age along the western branch, including the Malawi segment, is consistent with regional interpretations of southward propagation of the EARS (Ebinger et al. 1993; Flannery and Rosendahl, 1990). The half-graben structures are bound by ~100km scale border faults thought to follow the regional

foliation patterns of the basement rock (Ring et. al 1992). The northernmost Karonga Basin is bound to the east by the west dipping Livingstone Border Fault System (LBFS) which produces the high relief footwall escarpment known as the Livingstone Mountains (figure 1).

This Livingstone Range is composed of high grade crystalline metamorphic rocks (figure 2) that rise ~2km above modern Lake Malawi. There is little to no alluvial buffer between the modern shoreline and the western margin of Livingstone Mountains which marks the location of the LBFS. Bedrock channels dissecting the Livingstone Mountains therefore drain directly to the modern lake. There is a prominent divide ~8km east of the LBFS that is only crossed by two transverse drainages, leaving smaller drainages to climb the entire 2km of relief over relatively short horizontal distances (figure 3, 4).

The known tectonic history of the Karonga is mainly derived from analysis of seismic lines beneath Lake Malawi. One radiometric date exists on a welded tuff north of Lake Malawi overlaying early rift derived sediments establishing a minimum age for the onset of rifting at 8.6 Ma (Ebinger et al, 1989) which likely predates the establishment of a continuous border fault system and associated relief. Sedimentary sections from seismic lines indicate ~6km of throw has been accommodated along the LBFS (Ebinger et al, 1999) that initiated between 8-12 Ma (Mortimer et al., 2007) and accelerated by 6-5 Ma (Flannery and Rosendahl, 1990). A series of west dipping synthetic intra-basin faults have developed in the hanging wall of the rift valley to accommodate flexure associated with slip along the LBFS (Mortimer et al, 2007; Ebinger et al, 1987) which are still active and present an ongoing seismic hazard (Biggs et al, 2009). A shift from orthogonal to

oblique rifting ~0.5 to 0.4 Ma resulted in the nucleation of transform structures within the basin adjacent to the LBFS and counter-clockwise rotation of the Karonga Basin (Mortimer et al, 2007).

Directly south of the Karonga basin lies the Usisya Basin and associated Usisya Border Fault System (UBFS) (figure 1). Seismic analysis of the UBFS within Lake Malawi has interpreted the LBFS as a series of three major normal fault segments (Contreras et al., 2000). The high relief escarpment is located adjacent to the central segment of this fault system. The northern and southern segments are located offshore and their footwall blocks are below the lake surface and sediments. Two way travel time seismic reconstructions of slip along the central segment also show that along strike cumulative displacement can be loosely described as theoretical elliptical slip distribution (Contreras et al., 2000; figure 5). The footwall escarpment created by the central segment exposes the same high grade crystalline metamorphic which are present throughout the Livingstone Mountain escarpment. Behind both of these escarpments there is an extensive, relatively low-relief high-elevation landscape that is generally recognized as a remnant of an ancient erosional surface. (King L.C., 1963; Van Der Beek et al., 1998).

Modern Climate

Modern climate patterns in the Lake Malawi watershed are dominated by the interaction of the Inter-Tropical Convergence Zone (ITCZ) with the physiographic expression of the rift valley. The ITCZ is a zone of high precipitation that occurs at the convergence of warm equatorial air masses. In East Africa, the ITCZ migrates south over the Malawi Rift during austral summer creating monsoonal rains sourced from warm

Indian Ocean air masses from the south. While the strength and position of the ITCZ through the Quaternary is responsible for periodic aridification of the Malawi watershed (Johnson et al, 2002; Scholz, 2007) the modern monsoonal system represents a "wet" end-member state.

Despite the relatively high modern precipitation rates, orographic effects produce strong climatic gradients. The rift valley structure functions as a funnel for prevailing northward blowing monsoonal winds and portions of rift flank escarpments intercepting these winds are characterized by high rainfall, upwards of 2 m/yr, while areas in enclaves commonly experience less than 0.5 m/yr of rainfall (figure 4). For this reason, modern rainfall rates in the Livingston Mountains vary from ~2.5 m/year in the northern portions of the range to less than 0.8 m/yr in the south (Bookhagen, in review). Given the persistence of rift flanks and the well-described monsoonal climate pattern, it is reasonable to assume that these climatic gradients are persistent during wet periods, although the magnitude likely varies in response to the strength of the monsoonal system. However, during times of aridity the lack of moisture in the system will muffle any perceived orographic precipitation gradients due to a general lack of moisture in the environment. Rainfall along the UBFS is much less variable due to its positioning within the rift system. The UBFS is located in the center of the basin so moisture is not funneled towards one end as with the LBFS. There are also no areas of high topography in the windward direction creating a rain shadow over any portion of the escarpment. These conditions lead to less variable rainfall along-strike (1.5-2 m).

Paleoenvironmental Record

Numerous paleoenvironmental studies have been conducted in northern Malawi yielding a high resolution paleoclimatic record and a unique opportunity to link geomorphological observations with the lake basin's history. In 2005, the Lake Malawi Drilling Project successfully recovered over 600m of drill core from two locations, one in the the Karonga Basin adjacent to the LBFS and another from the Usisya basin adjacent to the UBFS, which record the environmental history of the basin and surrounding watershed extending back ~1.2 Ma (Scholz et al, 2006, 2011). Currently analysis of the shorter Karonga core provides a quantitative description of lake level, paleotemperature, paleoprecipitation, paleolimnology and watershed vegetation at high resolution (10-100 yr) extending to ~145ka (Cohen et al., 2007; Scholz et al., 2007; Brown et al., 2007; Beuning et al., 2011; Lyons et al., 2011; Stone et al., 2011; Woltering et al., 2011;). Analysis of the longer core, which extends into the Early Pleistocene, is still underway, but also contains a clear and interpretable paleorecord.

Observations from drill cores are complemented by existing seismic reflection data collected throughout the mid-1990s and early 2000's (e.g., Scholz, 1995; Mortimer et al., 2007). Shoreline reconstructions from stratigraphic analysis of seismic profiles by Lyons et al. 2011 agree with shallow water indicators recorded in the drill core studies and add spatial context to these findings. Together, these datasets have documented a series of three short-lived lake lowstands between 80-160 ka where lake level was ~500m below modern levels. These low stands are attributed to disruption of the modern monsoonal system resulting from procession driven changes in mean insolation during periods ofhigh orbital eccentricity (Lyons et al, 2011; Scholz et al, 2011).

CHAPTER 3

METHODS AND THEORY

Fault Displacement Theory

Theoretical models predict various displacement patterns along faults which have been substantiated with field observations. While these models describe reverse, normal and strike-slip faulting equally, the intended focus here is to understand displacement patterns along extensional normal faults. Expected patterns for a single normal fault rely heavily on the behavior of the fault tips. If the fault tips are allowed to advance uninhibited then the expected total displacement of the fault is predicted to be bow-shaped (figure 6). This pattern is created fault tips advance in proportion to total displacement along the fault (Cartwright et al., 1995; Walsh et al., 2002). If fault tip propagation is impeded on both sides then the total displacement will be elliptical due to the rapid transition to zero slip at the tips (Manighetti et al., 2001). Lithologic changes or interaction with transform structures related to the rotation of the Karonga Basin (Mortimer et al., 2007) are two possible examples of barriers to fault growth. These two end-member scenarios can be combined in any combination (temporally and spatially) to produce more complex displacement patterns.

Measurements across a variety of lithologic and tectonic settings have documented a power-law relationship between maximum displacement (D) and fault length (L) for faults greater than 100m length where D scales with $L^{1.4}$ (e.g., Davis et al 2005). One source of scatter in this relationship results from the dynamics of interacting fault strands. Cartwright et al. 2000 showed that when two growing normal faults link together the result is an anomalously low D:L ratio. By linking together, these faults

effectively become less restricted, similar to a fault that is allow to grow uninhibited (figure 6). After linkage, the discrete increase on L is followed by increased total displacement until the D:L ratio is restored. There are two end-member scenarios which can achieve this: 1) After linkage, fault tip propagation slows while displacement along the fault continues at a background rate or 2) The displacement rate along the entire fault accelerates in response to reduced resistance to strain. Observations from failed Jurassic rifting in the North Sea recorded an acceleration of slip rate along major fault strands after linkage and focusing of strain within a narrow field along the rift axis (Cowie et al 2005). All other things equal, it is logical that the slip rate a long a given fault will be greater if regional strain is focused along that fault (as opposed to numerous smaller faults).

The two end-member models of cumulative fault displacement based on fault growth mechanisms (figure 6) are limited in their real world applicability. Non-uniform lithospheric properties and tectonic stresses ensure that faults will behave neither as purely restricted nor unrestricted along their entire trace. Additionally, the presence of other faults distributed across a landscape will affect the displacement for any individual fault (Dawers and Anderson, 2000). These factors combine to produce cumulative displacement patterns such as those observed along the UBFS (figure 5). Importantly, this study does not seek to directly measure along-strike displacement patterns as the link between footwall uplift and displacement is unclear. Along-strike topographic observations will only match cumulative displacement if footwall uplift reflects cumulative displacement at each point along the fault. This is a reasonable starting

assumption that could be incorrect for a variety of reasons such as uneven loading of the hanging wall or isostatically induced uplift from focused erosion of the footwall.

Longitudinal Profiles and Channel Steepness Index

In equilibrium landscapes, channel gradients are a result of processes governed by parameters that vary systematically downstream such as discharge and channel width as well as regional conditions such as climate, lithology and uplift. This implies that if systematic longitudinal variations in channel gradient can be corrected for, then this normalized channel gradient can be used to interpret spatial and temporal variations in these regional parameters. Because rock type may be characterized via geologic mapping, this approach is ideal for investigating climatic and tectonic patterns of denudation.

Early work by Wolman [1955] recognized a negative power law relationship between channel slope (S) and discharge (Q):

$$S = tQ^{z}, \tag{1}$$

where *z* and *t* represent the rate of change in channel slope with discharge and the absolute magnitude of channel slope for a given discharge respectively. This is an expression of the familiar concave-up from of equilibrium channels where channel slope is reduced as you move down the system. Implicit in this expression is that while discharge exerts a first order control on channel slope, other parameters later identified as climate, lithology, uplift and physical process dominance (plucking, abrasion, cavitation) modify this relationship. The limited availability of discharge data further limits the utility of this model in systematically relating changes in slope to these various parameters.

Fortunately, discharge increases predictably with distance downstream as drainage area (A) increases. The relationship between discharge and drainage area can be described as:

$$Q = aA^x, \tag{2}$$

where the coefficient a is proportional to runoff per unit area and x is typically less <1 due to the non-linear scaling of gains, losses and storage with basin size (Flint 1974). This relationship is particularly useful in river incision models as drainage area is easily acquired via widely available digital elevation model (DEM) products because discharge data are limited to a small proportion of gaged river systems. Combining equations 1 and 2 yields equation 3 which relates channel slope and drainage area, two morphometric parameters that can be easily obtained through remotely sensed products.

$$S = (ta^z)A^{xz}. \tag{3}$$

The form of equation 3 allows for analysis of variation in slope vs. area across various landscapes but its purely empirical evaluation provides no context for the meaning of this variation. This lead to the development of the unit stream power model (Howard and Kerby, 1983; Whipple and Tucker, 1999; Whipple 2004) which combines first order principles with empirical observations relating basal shear stress, erosion, discharge and bed roughness. In its simplest form, it can be expressed as:

$$E = KA^mS^n, \tag{4}$$

where erosion (E) is a function of channel slope and drainage area to the n and m powers respectively. The coefficient K, often referred to as "erosional efficiency" is an amalgamation of various other parameters that characterize the erosional dependence on lithology, hydraulic roughness and geometry, and climate. In equation 4, drainage area

serves as a proxy for discharge and the exponents *m* and *n* reflect the differential dependence of river incision on channel slope and area. In a steady-state landscape, where uplift is balanced by erosion ($U = E$), equation 4 can be expressed as 5a:

$$U = KA^m S^m, \tag{5a}$$

$$S = \left(\frac{U}{K}\right)^{1/n} A^{-m/n}, \tag{5b}$$

$$S = k_s A^{-\theta}. \tag{5c}$$

Equation 5a can subsequently be rearranged to relate channel slope (*S*) to drainage area (*A*) (5b). Note the similarity between equation 3 and 5b; the coefficient (ta^z) and exponent xz is analogous to $\left(\frac{U}{K}\right)^{1/n}$ and the ratio m/n respectively. While equation 3 is relates *S* and *A*, the relationship derived from the stream power model (5b) specifies a dependence on uplift (*U*), climate & rock resistance to erosion (*K*), and incision mechanics (*m* and *n*). While the exponents m and n are free parameters, field observations of the ratio of *m/n* have shown that values typically fall between 0.4 and 0.6 and are independent of climate, tectonics and lithology (Howard and Kerby, 1983, Snyder et al., 2000) which is consistent with theoretical expectations (Whipple and Tucker, 1999). Additionally, the coefficient $\left(\frac{U}{K}\right)^{1/n}$ is thought to be constant if climate, lithology and uplift are uniform for a given drainage basin. With these observations in mind, we express the ratio of *m/n* as Θ and the coefficient $\left(\frac{U}{K}\right)^{1/n}$ as k_{sn}, which we call the reference concavity and channel steepness respectively, to form equation 5c.

Because the typical values of Θ fall between 0.4 and 0.6 and are independent of the parameters imbedded in k_s, it is often appropriate to assume a fixed value of Θ across different catchments in order to quantify a normalized channel steepness, ksn. In this analysis, I selected a value of 0.45 for Θ based on best fits of longitudinal profiles. Variation of ksn in different basins or within the same basin therefore implies variation in the uplift, climate and/or lithology. Selecting catchments with minimal variation in rock type can further simplify the analysis and ksn becomes a valuable tool in characterizing uplift or climate patterns. Because either higher uplift rates ($\uparrow U$) or a less efficient climate ($\downarrow K$) result in higher ksn values, a more in depth analysis of these patterns with regards to tectonic structures and climate patterns is needed to further constrain the forcing. Furthermore, in steady state when uplift is balanced by erosion ($U=E$), tectonically derived variation in ksn will be accompanied by variation in erosion rates while climatically induced variation in ksn will not.

By using channel steepness to interpret variation in uplift rates along fault traces, we can learn about the growth and maturity of fault systems. The two end member fault growth models discussed in the previous section (restricted vs. unrestricted) have different along-strike uplift patterns. In the restricted model, because there is no slip at the tips between two hypothetical time steps, the uplift rate (length / Δ time) toward the fault tips goes to zero (figure 6) and therefore ksn will decrease towards the end of the fault. The ability to resolve this behavior towards the fault tips will depend on length scale over which this decrease occurs. If cumulative displacement and uplift are linked, then the extent of the UBFS escarpment should be record this behavior in the central segment of the fault (figure 5).

If U or K (uplift or erosional efficiency) change at any time, along any stretch of the faults evolution then there will be a discrepancy between channel steepness values within each longitudinal profile. The transition between these two channel steepness is referred to as a knickpoint. The elevation pattern of knickpoints in the system can be used to further constrain whether or not changes in ksn as described above are due to tectonic variations. If numerous knickpoints are present along-strike and they are assumed to be the same age, their elevations will be proportional to the along-strike uplift rate which is proportional to ksn. If the knickpoint elevations do not mirror changes in ksn then either 1) the contemporaneous assumption has been violated 2) the variation in ksn is caused by a change in erosional efficiency or 3) the fault growth is unrestricted at the tips and therefore a suite of knickpoints along-strike will all experience the same uplift. Careful assessment of all structural and environmental constraints will be required to differentiate between these plausible scenarios.

CHAPTER 4

RESULTS

Livingstone Border Fault System

Channels analyzed along the Livingstone Border Fault system satisfied a number of pre-conditions to ensure that there is sufficient spatial coverage to test hypotheses and factors affecting channel steepness not related to tectonics or climate were minimized. All channels crossing the trace of the LBFS with a drainage area of over 2.5km^2 were selected and in the case of larger drainages, multiple tributaries were included in the analysis. The NW edge of the analysis is bound by termination of the continuous escarpment in the Rungwe Volcanic Region and the SE extent is limited by a lithological between crystalline Precambrian basement and Permian-Triassic Karroo beds (Figure 2). This lithologic transition also corresponds to the accommodation zone between the west dipping Livingstone Border Fault System and the East Dipping Usisya Border Fault. The majority of analyzed channels are small (less than 10km length, 25km^2 drainage area) because they do not transverse the drainage divide 8 km NE of the LBFS trace.

Four evenly spaced transverse drainages cross the escarpment drainage. All three drainage networks show patterns suggestive of significant pre-rift topographic controls as well as structural controls related to rifting. The distance between the eastern lake margin and the eastern edge of the Lake Malawi watershed, including the area draining the Livingstone Mountains, is narrower than the same distance between the western lake margin and western watershed boundary. This is consistent with the generally SE dipping orientation of the regional low-relief erosional surface (King, 1955). The Karonga Basin shows the greatest deviation from this regional pattern. Because this basin is oriented

NW-SE as opposed to N-S there is greater likelihood that that the watershed could grow through drainage capture in this region. Additionally, the Malawi portion of the east Africa rift becomes younger to the south (Chorowicz et al., 2005) so northern rift flanks will have had more time to develop drainage networks. Finally, the largest deviation in watershed boundary width occurs along the eastern watershed boundary occurs adjacent to the accommodation zone between the Karonga and Usisya Basin where the Ruhuhu river system has excavated a valley within relatively easily erodible Karoo deposits from within a paleobasin (figure 2).

At a finer scale, the northern and southern transverse drainages show a bias in channel upstream bifurcation towards the north and south respectively. These tributaries follow the orientation of basins bound by Jurassic structures that have been reactivated for some duration during the modern rifting event. The middle (and largest) transverse drainage system displays a more regular dendritic pattern while the northern and southern transverse drainage tributaries are both asymmetric in their drainage patterns (figures 3,4). These patterns may be influenced by landscape dynamics before rifting or are potentially related to early rifting dynamics.

Despite differences in drainage organization, specific features of channel profiles are consistent between all three transverse drainage systems. Each drainage and its associated tributaries display profiles with a prominent knickpoint separating a steep lower reach from a relatively low gradient upper reach. Representative and geographically diverse examples of these profiles are represented by channel profiles 23, 39, and 57– corresponding to a northern, central, and southern transverse drainage respectively (channel locations – figure 3, longitudinal profiles – figures 7, 8, 9). While

these large drainages also contain numerous other knickpoints and steepness variations, they all can be characterized by this prominent knickpoint (located at ~2000m for channel 23 and ~1500m for channels 39 & 57). Other features in the profiles above and below this knickpoint can likely be attributed to a variety of unknown sources poorly constrained structural complications and the potential for variability within the coarsely mapped Archean basement rocks. These complications will not be further explored here because these unknowns and the coarse resolution of the topographic data would limit the potential of any such analysis. Also, due to these complications, comparing the absolute values of ksn is only helpful in illustrating that the steeper reaches beneath the knickpoint are generally characterized by ksn values >300 and ksn values above the knickpoint are less than 100. Convexities and well-defined knickpoints within this steeper reaches visible in profile #23 & #57 (Figure 4 & 6) may be geomorphically significant but difficult to interpret from the limited sample of large transverse drainages.

The smaller mountain front drainages crossing the LBFS are responding to the same regional geomorphic forcing of uplift along the LBFS without the compounding factor of draining large portions of the low-relief erosional. Only catchments between 4 and 25 km^2 will be discussed with regards to rangefront channels in order to eliminate sources of uncertainty related to variation in drainage area. 53 rangefront channels that meet these criteria, providing sufficient coverage across the entire border fault system (~1 channel / 3.5 km along-strike distance) to detect along strike topographic variations responding to the regional scale tectonic and climatic patterns identified. Similar to the larger transverse drainage systems, nearly all of the rangefront drainages of sufficient size contain at least one major knickpoint. Channel profiles 25, 28, 50, 63, and 67 (figures 10

- 14) are examples of channels that show clearly interpretable longitudinal profiles yet illustrate well the variability of channel morphologies in the region. Profiles 25, 28, 50 & 63 all have a single knickpoint separating a steeper lower section form a gentler sloping upper section but this knickpoint occurs at elevations ranging from 1000m on profile 50 to 1700 meters on profiles 28 and 63. One challenge in interpreting these longitudinal profiles is determining which knickpoints are correlative, especially because some channels such as 67 show multiple knickpoints (figure 14). Relying on ksn values or knickpoint elevation patterns to correlate steepened sections is not an option as patterns of changing ksn and/or knickpoint elevations encode valuable geomorphic information. Therefore initial results are plotted and interpreted by correlating channel reaches and knickpoints using a "bottom-up" approach where the lowest knickpoints on each channel are considered contemporaneous.

This approach simplifies interpretations because channels adjust from the outlet to the headwaters. Therefore a "bottom-up" interpretation results in the comparison of most recent conditions at one part of the fault to most recent conditions at the other. This does not assume that the geomorphic setting is constant spatially along the entire stretch of the analysis nor does it assume the absolute timing of changes is the same, only that we are comparing the "youngest," "2^{nd} youngest," "3^{rd} youngest" portion of each channel respectively, etc.. This allows for a spatial analysis of variations in channel morphology which can be compared to expected patterns induced by tectonics and climate. If spatial patterns are recognized only then can specific knickpoints and channel reaches be correlated temporally. For example, if knickpoint elevations reveal an elliptical

displacement field then this data supports the notion that these features are systematically related temporally as part of an evolving fault strand.

Organizing the results in this manner allows for the plotting of knickpoint elevations and ksn along fault strike. The most complex rangefront channel profiles contain two knickpoints and therefore three associated channel reaches. From the "bottom-up" these features are referred to as Ksn1, KP1, Ksn2, KP2, and Ksn3 respectively. Viewing the knickpoint elevations and ksn values of these five features along-strike of the 180km long study area reveals several first order patterns as well as significant scatter. From 0-70km along strike, ksn1 values are constant averaging ~150 albeit with a spread of +/- 50 when not including outliers (figure 15). The significance and source of these outliers will be discussed later in this section. From ~70-80km along strike, Ksn1 values increase to ~300 before slowly declining towards the southern end of the study region. This increase corresponds to an along-strike distance approximately 30km south of the northernmost extent of Lake Malawi midway between the central and southern transverse drainage systems (figure 15). While the transition to higher ksn values is clearly visible it cannot be determined precisely over what distance this transition occurs due the significant scatter in the data. It is also notable that at ~40km and ~110km are two groupings of significant outliers.

This pattern shows no correlation to the elevations of KP1, values of Ksn2, elevations of KP2 or values of Ksn3. From north to south KP1 shows a pattern of rapidly decreasing elevations until ~50km and then slowly decreasing thereafter (figure 15). However, if the outlet elevation of each channel is subtracted from KP1 elevations the relationship flattens out significantly (figure 16). This 50km-along-strike transition point

corresponds to the northern shore of Lake Malawi where the shoreline follows the trace of the LBFS. Above these knickpoints (KP1) is the reach of channel characterized by Ksn2 (figure 17). Values of Ksn2 are lower than Ksn1 and generally lie in the range of 75-150. These values also show that there are two humps of higher Ksn values accompanied by lows at 60km along-strike and towards the southern end of the analysis. These two areas correspond to the large central transverse drainage system and accommodation zone between the Livingstone and Usisya fault systems respectively. Knickpoints above Ksn2 (KP2) linearly decline to the south (figure 17). Only a limited number of the rangefront drainages express KP2 so figure 17 includes KP2 elevations from catchments >25km^2. Because of the large drainage area discrepancy between the rangefront and transverse system, data points are no longer scaled to drainage area. Note that this trend in knickpoints compares favorably to the regional slope of the low-relief erosional surface located behind the escarpment. Finally, in the most upper reaches of the rangefront and transverse channels, Ksn3 shows no discernible trend besides remaining low (<100) (figure 18).

While the density of the dataset allows for clearly expressed trends, significant deviations do exist. A more detailed look at the longitudinal profiles of channels in these areas can reveal whether the source of these deviations is related to the methodology, geomorphology or both. Significant deviations occur in the form of anomalously high Ksn1 values at 35-45km and 105-115km along strike (figure 16). Ksn2 values can be described as having a few scattered extreme outliers in addition to numerous anomalously low values that result in a large spread relative to the absolute values (figure 17). KP1 elevations also show increased scatter between 80-130km along strike (figure 13). By

definition, channel reaches of differing ksn are separated by knickpoints, so methodological errors in identifying and correlating these features will affect the measurement (elevation, steepness value) of all the features for a particular channel.

Results from manual fits of longitudinal profiles are also consistent with objective measures of topography and automatically generated Ksn maps. Automatic Ksn maps are generated similar to manual fits by assuming a constant reference concavity. However, instead of characterizing long stretches of channels chosen by the user with one steepness value, auto Ksn maps are generated by dividing each channel into equal increments (in this case 500 m) and calculating the channel steepness for each increment independently. This approach is beneficial in that it is objective but often subtle details can be missed or noise can be over interpreted. Nearly every channel in the automatic Ksn map has a steeper lower reach and gentler upper reach (figure 17) although the knickzone between the steeper lower reach and gentler upper reach occur further from the outlet in the transverse systems. Measures of local relief (2.5km radius) reveal two elongated regions of high relief along the LBFS separated by a low relief section near the central transverse drainage system at 60km along-strike. Relief also decreases towards the NW and SE tips of the fault system. This pattern is consistent with the two humps of higher Ksn2 values found above the knick points.

Usisya Border Fault System

A similar approach was taken to organizing the results from the Usisya Border Fault system. The Usisya Border Fault system, like the Livingstone Border Fault System, also creates a fairly continuous high relief escarpment that defines the lake margin.

Unlike the Livingstone escarpment, there is not a well-defined drainage divide proximal to the lake margin that creates a clear distinction between the rangefront and transverse drainages. There are also less clearly defined bounds to the study area as both the northern and southern margins of the escarpment transition into accommodation zones without any natural topographic or lithologic boundaries (figure 2). Because of this the extent of analyzed channels is limited to bedrock channels flowing directly from the Usisya escarpment into Lake Malawi. This limits the along-strike length of the analysis to ~120km. While there are still high relief areas to the north and south of this defined area, structural complications and broad alluvial plains confound along-strike comparisons of profiles beyond this 120km wide zone.

Because there is not a clear drainage divide that closely mirrors the lake margin atop the Usisya escarpment, the distribution of drainage sizes is significantly different than the previously described Livingstone system, making it difficult to isolate drainages of similar size to compare along strike. After measuring all channels draining into Lake Malawi from the Usisya escarpment, it was determined that isolating channels between 2.5-40 km^2 yielded enough remaining channels to provide data coverage along the entire escarpment without including the larger systems that may respond differently because they integrate drainage area from behind the Usisya escarpment that experiences different mean annual rainfall. This strategy yielded 38 channels along the 120km stretch.

Individual longitudinal profiles for this study area are characterized by many of the same features that are ubiquitous in the Livingstone channels. Specifically, nearly every channel contains a prominent knickpoint separating high channel steepness values from low. The higher channel steepness values are also below the knickpoint. Unlike the

Livingstone channels, longitudinal profiles from the Usisya Border Fault system do not commonly contain an upper knickpoint. Along-strike analysis channel steepness values and knickpoint elevations reveal patters that differ from those observed along the Livingstone border Fault system.

Channel steepness values in the lowest reach of Usisya channels (Ksn1) are approximately steady from 0-90 km along-strike before they fall dramatically toward the southern end of the study area (figure 19). Although highly variable, the ksn values between 0-90km are typically in the range of 100-200. After 90 km along-strike, values quickly fall to over the next 30 km to values less than 50. A visual analysis of the knickpoint elevations (KP1) above Ksn1 clearly shows low elevations along the southern end of the border fault (90-120 km) that correspond to the locations of the low Ksn1 values (figure 19). The pattern over the northern 2/3 of the system is less clear. Between 0-90 km along strike, the available data shows two separate highs centered 30 and 80 km. However, since not all channels have knickpoints, the coverage of KP1 elevations over the entire escarpment is less continuous than Ksn1 and not sufficient to clearly interpret these patterns. For the purpose of assessing the validity of the KP1 patterns we can plot KP1 vs Ksn1 for each longitudinal profile. There is a correlation between the knickpoint elevations and channel steepness which suggests that KP1 elevations likely mirror the pattern and variability observed in the more dense Ksn1 dataset. This correlation is also suggestive of a driver for the channel steepening and knickpoint development that will be addressed in the discussion section. Finally, the upper segments of the channels (Ksn2) are described by steepness values that are uniformly lower than ksn1. Ksn2 values range between 10 & 110 and don't show any systematic variation along strike (Figure 20).

CHAPTER 5

DISCUSSION

Livingstone Border Fault System

There is more than one plausible interpretation of the transient channel features described in the previous section. Along-strike patterns of individual features (Ksn1, KP1, Ksn2, KP2, Ksn3) further constrain the plausible forcings and consideration of relationships between Ksn and KP elevations allow for the most robust interpretation of data. Plausible alternative interpretations considered here assume that a single forcing is responsible for the pattern observed at each of the three individual timesteps (Ksn1, Ksn2, Ksn3). This is an appropriate simplification for this study as we are concerned with first-order tectonic or climatic controls and in specific instances it is reasonable to assume that one of these two forcings is constant. The possibility of two of these working in concert with each other will be discussed after investigating this baseline assumption. Each plausible tectonic and environmental forcing will be carefully explored below but the best possible interpretations based on available data are briefly summarized in table 1.

The observed knickpoints and channel steepness variations for a single representative channel in this study can be explained by an increase in uplift or a decrease in erosional efficiency (K) because we think there is no systematic variation in lithology. Since each channel reach is separated by a knickpoint these changes must have been discrete. Extending this interpretation to the entire network of rangefront channels, the pattern of Ksn1 previously described represents either uplift or climate patterns preserved in the topography along the 180km long escarpment. If uplift patterns are responsible,

Table 1: Summary of preferred interpretations from stream profile analysis. All portions of both the Livingstone and Usisya Border Fault Systems were primarily influenced by tectonics (albeit different styles) with the exception of Ksn1 from the Livingstone Border Fault System.

	CHANNEL SEGMENT	IMPLIED UPLIFT PATTERN	CLIMATE IMPRINT?	DESCRIPTION / INTERPRETATION
LIVINGSTONE BORDER FAULT SYSTEM	Ksn1	--	YES	increase in Ksn1 values correlate with decrease in MAP
	KP1	~constant OR gentle decrease to the south	NO	steady uplift rate along entire system, potentially indicates accelerated uplift initiated in the NE
	Ksn2	2 segments	NO	2 ~elliptical channel steepness patterns imply gradient in paleo uplift patterns
	KP2	--	NO	knickpoint elevations correlate with slope of pre-rift erosional surface
	Ksn3	early rifting	NO	no resolvable pattern and high variability consistent with distributed extensional faulting
USISYA BORDER FAULT SYSTEM	Ksn1	1 partial segment	NO	correlation between Ksn1 and KP supports uplift pattern
	KP1	1 partial segment	NO	correlation between Ksn1 and KP supports uplift pattern
	Ksn2	early rifting	NO	no resolvable pattern and high variability consistent with disperse extensional faulting

assuming a constant climate forcing, then the increase in ksn1 between 70-80km would represent an increase in uplift rates to the south at this location of the border fault system. Alternatively, if uplift rates along the fault system have been constant then the pattern could be explained by a shift to a drier, less efficient climate resulting in higher Ksn1 values. Climate may also play a role in setting the steepness of the lowermost channel reach by modulating base-level via lake level. If low-lake conditions have been persistent long enough to be geomorphically significant then locations where the bathometric slope is greater than the channel slope will have experienced recent incision and steepening. The likelihood of each of these drivers controlling ksn patterns can be evaluated by comparing the measured along-strike ksn patterns to the region's documented tectonic structures, bathymetric slope and rainfall patterns.

A significant change in uplift rates along the Livingstone Border Fault footwall implied by the channel steepness values requires a structural segmentation of the border fault system or along-strike flexure of the uplifting footwall. Relay zones located at ~90 & 135 km along-strike (figure 15, 17) do not correspond to the increase in Ksn1 values. Mortimer et al. 2007 mapped three intrabasin structures striking perpendicular the LBFS, two located near the aforementioned relay zones and another adjacent to the large central transverse drainage. These dip-slip structures are inferred from analysis of sedimentary packages within the hanging wall of the fault with no indication that they cross-cut the main trace of the Livingstone Border Fault. All three of these of these NE-SW striking structures are downthrown to the NE and were activated during the most recent phase of rifting. Therefore if slip along these structures is directly translated to variation in uplift rates along the footwall then systematic increases in Ksn1 should correspond to upthrown

footwall blocks. The increase in Ksn1 values that occurs between 60 and 80 km along strike loosely correlates with the northernmost of these structures located ~70km along strike. While the general pattern is consistent with segmentation of the main border fault, the pattern is not completely consistent because 1) the increase in Ksn1 values appears more gradual than the sharp increase expected by segmentation and 2) there are no visual indications that this structure extends beyond the hanging wall in the form of altered drainage patterns or linear topographic features. Furthermore, this correlation is not observed in the other two NE-SW striking hanging wall structures. Most definitively, the elevation of KP1, marking the transition between Ksn1 and Ksn2, is set by the product of uplift rate and time since the onset of uplift. If variation in Ksn1 is indeed reflecting spatial variation in uplift rates then this pattern would also be reflected in the elevations of KP1. KP1 elevations show significant noise between 80-120km along strike but do not increase across proposed structural segmentation at ~70km.

To assess the potential impact of incision via climatically modulated base-level on Ksn1 we can simply compare predicted patterns to observed patterns for a known base-level history. During lake high stands, which are similar to the modern lake level, baselevel for footwall channels to the NW between 0-50km along-strike is set by the elevation of the axial alluvial plain relative to the footwall. SE of 50km along-strike where footwall channels flow directly into Lake Malawi baselevel is set by the elevation of the lake surface. Barring adjustments to lake level or the alluvial system, incision of footwall channels is controlled purely via border fault slip and the erosional efficiency of upland landscapes. Importantly, Lake Malawi also sets the baselevel for the axial alluvial plain so a change in lake level will affect footwall channels grading directly into the lake

in addition to those emptying onto the alluvial plain. As lake-level falls and channels extend further into the basin, the behavior of these channel systems will be controlled by the gradient of the newly exposed land surface relative to the channel gradient of the existing channels (Snyder et al., 2002). If the gradient of the newly exposed land surface is greater than the existing channel then a pulse of incision will propagate upstream but if the gradient is lower aggradation will ensue. The gradient of the newly exposed land surface can be estimated by measuring the line of steepest decent in the lake bathymetry. Importantly, the exposed bathymetric slope will vary along-strike and therefore any footwall incision driven via this process will reflect this along-strike pattern. The bathymetric gradient between footwall channels and the lake lowstand shoreline increases steadily towards the SE (figure 21 - top). If this driver is geomorphically significant, Ksn1 would show an inverse pattern of steadily increasing steepness towards the SE. The observed patterns of decreasing values from 80km along-strike towards the SE end of the study area are opposite of this expected pattern, showing that the effects of climate induced lake fluctuations are not geomorphically significant in this location. This is unsurprising in that 1) documented megadroughts are short-lived (Scholz et al 2007) 2) aridity of this magnitude is likely accompanied by slower landscape response times and 3) to date there is no evidence of longer-term acidification before 200 kya.

In the absence of tectonic or lake-level controls on Ksn1, spatial gradients in climate may be imprinted on the landscape if modern patterns have been persistent over geomorphic timescales. The modern climatic gradient along the Livingstone Rift Flank generally goes from high mean annual rainfall in the NW of the range (up to 2.5 m/year) and lower MAP in the SE (as low as 0.8 m/year) as quantified by the TRMM data. The

transition from high to low rainfall along the rift flank occurs gradually over a distance of ~80 km along strike as represented by the 12-year TRMM averages. Figure 21 shows the 20 km moving average along-strike TRMM MAP within 8 km of the shoreline. Higher frequency variation imprinted on top of this gradient can be accredited to the relatively coarse 4km resolution of the TRMM data compared to the size of range front channels and distance to the drainage divide. A moving average was calculated as it is unlikely that the high frequency variation in MAP would be persistent over geomorphic timescales. Notably, the visible increase in Ksn1 values is roughly correlative to the decrease in MAP along the rift flank. Given noise in both the TRMM and channel steepness data it is difficult to determine how quickly the transition between wet & less steep channels in the NW to dry and steeper channels in the SE occurs. The transition between wet and dry rift flank conditions occurs at approximately 80km along strike. Spatially averaged MAP NW of 80km is ~1.8 m/year while SE of 80km averages ~1.2 m/year. The average channel steepness values for these two halves of the rift flank are 214 and 267 respectively. This broad correlation between MAP and channel steepness in the lowest reaches of the channels (Ksn1) supports the feasibility of a link between climate and topography.

The spatial variation in MAP in the region results from moist monsoonal air interacting with the high relief of rift flanks. While the persistence of this rainfall pattern is undocumented, it is reasonable to infer that this gradient has existed since the development of high relief along a continuous border fault. Any preservation of this climatic gradient in the topography of the rift flank is therefore expected to be preserved in the lower reaches of the channels that are best adjusted to recent conditions.

Expression of this climatic gradient in higher reaches of the channels will only occur where the timescales preserved in these reaches are consistent with a high relief orographic barrier. Furthermore, because climatically induced channel steepening does not affect the vertical migration of knickpoints (assuming n~1 in equation 5b), any knickpoint caused by or above the climatically impacted zone will reflect uplift patterns along the rift flank since initiation of climatic steepening.

Knickpoint elevations above Ksn1 (KP1) have an along-strike pattern that is not consistent with the attribution of uplift as the primary driver of Ksn1 variation. This requires an alternative explanation for KP1 patterns and further supports the observation that rainfall patterns are only observed parameter that is consistent with observed Ksn1 variation. Interpreting patterns of KP1 elevations is complicated due to the variable outlet elevation for each channel. Because it has already been inferred that the coupled effects of lake-level fluctuation and bathymetric slope have little impact on Ksn1, we extend this observation to KP1 elevations and assume that the pattern of modern outlet elevations determined by the axial alluvial plain and modern lake level can be extended to the past. Subtracting outlet elevations from KP1 elevations reveals that KP1 elevations decrease subtly along-strike with reference to their modern baselevel (figure 16). Independently, this trend could be interpreted to represent a variety of spatial-temporal conditions such as 1) a spatial distribution of uplift rates 2) A temporal record of the transition between Ksn1 & Ksn2 (i.e. this change occurred first in the NW and propagated to the SE) or 3) an indication that the pattern of outlet elevations (baselevel) when the transition from Ksn1 to Ksn2 occurred was different from the modern.

Of these three possibilities, only two are consistent with the broader observations from the region. As previously discussed, channel steepness values from Ksn1 do not support the possibility of higher uplift rates towards the NW of the escarpment. However, spatially constant uplift rates that initiated in the NW and propagated towards the SE could produce the observed KP1 pattern without imparting variation in the channel steepness of the reaches below the knickpoint (Ksn1). Finally, if the gradient of the axial alluvial plain were steeper during the transition from Ksn2 to Ksn1, the gradient of channel outlet elevations would also be steeper than the modern. In this scenario, a spatially and temporally uniform acceleration of uplift would create a knickpoint at a uniform elevation above baselevel. Subsequent readjustment of the alluvial system to a lower gradient would result in a differential decrease in along-strike outlet elevations. Footwall channels emptying onto the alluvial plain towards the NE (farther upstream in the alluvial system) would experience the greatest outlet drop as a result of a lower gradient alluvial plain if regional baselevel remained constant due the geometry of longitudinal profiles. When comparing KP elevations to modern outlet elevations, this scenario would produce the observed decrease in relief between KP1 and modern outlet elevation. The plausibility that the axial alluvial system adjusted to a lower gradient is supported by incision in the alluvial plain and range front fan systems NE of 35km along strike. Topographic and satellite observations reveal that this incision is likely a response of drainage and basin integration between the Rungwe Volcanics and the main Karonga Basin. The lack of steepening in the lower reaches of footwall channels (Ksn1) is not consistent with this interpretation. However, if this incision is young relative to the age of KP1 then footwall channels would have little time to adjust and would simply contribute

to the noise that is common near the channel outlets along much of the Livingstone escarpment. Therefore it is plausible that adjustment of the alluvial plain, likely due to drainage integration, explains the patterns of KP1 and outlet elevations particularly between 0-35 km along-strike.

The channel reaches above KP1, quantified by Ksn2, preserve a morphology that reflects conditions predating those interpreted from Ksn1. KP1 represents the transition between these two conditions. The lower steepness values for ksn2 relative to ksn1 suggest an increase in slip rate (uplift rate) along the entire border fault system. Alternative explanations would require a large scale regional change in climate causing the landscape to adjust to a higher relief and less efficient landscape. To have created the clearly decipherable knickzone, this transition this would have had to occur over a discrete time interval and be of a large magnitude to contrast with the already highly variable climate in the region. Given the lack of evidence for a unidirectional climate change in SE Africa that meets these criteria (Brown et al, 2013), it is probably that the increase in channel steepness between Ksn1 and Ksn2 is a result of a uniform increase in footwall uplift rate along the entire border fault system.

A discrete increase in slip along the entire Livingstone border Fault system would require either an absolute increase in regional extension rates or a focusing of regional extension along the main border fault system. Without an acceleration of regional extension, focusing a greater percentage of slip along the LBFS is possible by the transfer of slip from nearby en echelon faults to the LBFS system. This behavior has been documented before in other extensional environments where individual fault segments link together and accommodate a greater proportion of the slip as they do (Cowie et al,

2005). While a widespread regional increase in extension rate is plausible, the along-strike variation in Ksn2 and described footwall drainage network patterns support the conclusion that slip accelerated due to the linking of individual segments of the Livingstone Border Fault System. This evolution is conceptually illustrated in figure 22 showing how transverse drainages will occupy zones between fault segments and entrench their positions once said segments link together. Furthermore, once these segments link together, the continuous fault created cannibalizes displacement from other adjacent faults since there will be a lower failure threshold along the more developed fault system.

The two along-strike zones of higher channel steepness above KP1 (Ksn2) are consistent with theoretical predictions of along-strike displacement for individual faults. As illustrated in figure 6, a gradient in uplift rate (and therefore a gradient in channel steepness) is expected to accompany a gradient in cumulative displacement so long as fault growth is restricted at the tips. Assuming the transition from Ksn1 to Ksn2 happened simultaneously along the entire fault system then the pattern of ksn2 can be used as a proxy for the local paleorelief of the system (Dibiase et al, 2010). It is notable that the modern 2.5km radius local relief closely mirrors the two zones of high ksn2 because the majority of relief within each catchment is above KP1 (figure 17) which is consistent with the relative knickpoint elevations bounding these channel reaches. In map view, these two zones of high relief are also striking at different orientations and are connected by a zone of low relief. This orientation is also consistent with the interpretation that during the time interval represented by Ksn2 the LBFS did not form a continuous high relief escarpment as it does today. Rather, at least two independent en

echelon normal faults adjacent to each other merged form the continuous system we observe today. During and before the time of integration, theory predicts that other en echelon faults would have existed but slip from them would be transferred onto the dominant Livingstone Border Fault System as it developed (e.g., Cartwright et al, 1995). Inactive en echelon faults that meet these criteria have been mapped within the hanging wall via analysis of seismic surveys (Mortimer et al, 2007) but it is unclear whether these structures accommodated early flexure of the hanging wall or a period of less localized extension. There are also old Jurassic structures east of the main Livingstone Border Fault system that clearly have been active since the onset of rifting based on their topographic expression.

Paleo-relief created by a segregated border fault system would also impart a legacy on the organization of footwall drainages as well as the location of basin depocenters (Cowie et al., 2006). The majority of footwall drainages are limited in size due back tilting caused by isostatic restoring stresses (Ebinger et al, 1993). The entire Malawi Rift also formed within the previously east-flowing erosional surface (King, 1955). Therefore, the transverse drainages along the Livingstone Border Fault System likely occupied their current along-strike locations before the development of a continuous border fault system. Drainages that charted their course and amalgamated drainage area during a time of less focused faulting would be more likely to keep up with uplift upon the initiation of a continuous border fault. Thus the along-strike location of these transverse systems likely occurs between individual faults before they linked into the continuous border fault system today. The largest of these transverse drainages crosses traverses the Livingstone Border Fault System at ~60km along strike which

directly correlates to the along-strike low in Ksn2. Within the hanging wall, sedimentation will be greatest where there is the greatest accommodation space next to individual fault segments (Cartwright et al., 1995). Seismic reflection data shows that the two segments proposed here based on terrestrial channel information match the location of early sequence basin fill and fault segment locations derived from (Mortimer et al, 2007).

Above Ksn2, KP2 elevations decline linearly and channel steepness values above this knickpoint who no systematic along-strike variation. A 10-km wide swath profile following the high, relatively flat terrain behind the rift flank closely mirrors this decreasing trend suggests that the terrain above KP2 is analogous to the more gently dissected and faulted terrain behind rift flank (figure 17). Because the environment represented by this portion of the longitudinal profiles likely preserves more widely distributed faulting associated with early rifting overprinting paleotopography (i.e figure 22), it is unlikely that any discernible pattern in along-strike channel steepness would be decipherable. If this interpretation is correct, then this means the topography of the rift flank produced by the Livingstone Border Fault system preserves a useful and interpretable record of rift basin evolution from its beginning stages to present that is in agreement with robust seismic reflection data and interpretation from the hangingwall.

Usisya Border Fault System

The environmental patterns along the entire stretch of the Usisya Border Fault system contrast with those previously presented and discussed along the LBFS. Observations from the LBFS support the presence of long lasting gradients in

precipitation and outlet elevation and bathymetry that overprint a tectonic signal that was poorly constrained before this analysis. While detailed analysis of the Livingstone system limited the plausible interpretations, the contrasting gradients along the Usisya Border Fault system present an opportunity to test the assumptions of this analysis within a different terrain. Along the Usisya Rift flank, the lack of a rainfall gradient coupled with the uniformly steep bathymetric slope, eliminate the expectation that anything other than tectonic patterns will be reflected in the along-strike observations.

If these assumptions are reasonable, the channel steepness from the lowest reach of longitudinal profiles, Ksn1, should follow trends consistent with documented structures and fault displacement theory. There are no visible or mapped secondary structures along the entire stretch of the UBFS analyzed here. Seismic observations from Lake Malawi suggest that the UBFS escarpment is the topographic expression resulting from the central of three fault segments (figure 5). The other two segments located directly north and south of the exposed escarpment are obscured by the modern water level and sediments of Lake Malawi (Contreras et al, 2000). The decreasing values of Ksn1 towards the southern end of the analyzed section are consistent with theoretical displacement patterns for a single restricted single fault system (figure 6) and the cumulative displacement patterns interpreted by Contreras et al (2000) from lake sediment thicknesses. In the case of the southern fault tip, topographic expression of the footwall escarpment as measured by channel steepness is in complete agreement with the displacement record, but this relationship is less definitive in the northern zone.

Along the central and northern portion of the escarpment, no systematic variation in ksn1 values is observable. Ksn1 over this range appears to be randomly distributed in

an envelope between 100-250. This could be a result of the accommodation zone between the Karonga and Usisya Basin truncating the northern edge of the escarpment and/or causing this section to behave more like an unrestricted fault segment where cumulative displacement does decrease towards the fault tip but uplift rate does not (figure 6). The slightly less elliptical shape to the cumulative displacement toward the northern edge supports this possibility. East dipping structures synthetic to the LBFS are also found ~30km from the northern edge of study area which may have cannibalized the northern tip of the UBFS.

The elevations of knickpoints above Ksn1 (KP1) further reinforce the interpretation that along-strike variation in Ksn1 is tectonically driven. Not all channels measured for Ksn1 contain a clearly identifiable knickpoint which limits the density and usefulness of along strike KP1 elevation data for the purpose of interpreting along-strike variation in uplift patterns (figure 19). However, the KP1 elevation data that is available reinforces the interpretation that patterns of Ksn1 are driven by variation in uplift along the escarpment. Plotting KP1 elevations against ksn2 values reveals that the two parameters are correlated with an R^2 value of 0.65 (figure 20). This is only possible if uplift rates are the primary driver of channel steepness variation as changes in erosional efficiency would not affect the elevation of knickpoints.

The low and highly variable channel steepness values above the knickpoint (Ksn2) evoke comparison to Ksn3 values in the uppermost reaches of LBFS channels. This pattern of highly variable and relatively low steepness is again consistent with what would be expected from unfocused extension and faulting during the earliest stages of rift development. Some of the randomness in channels steepness variation could also be a

legacy of pre-rift topography. In contrast to the observations from the LBFS, the UBFS contains one less knickpoint and therefore records one less time-step of rift evolution. The difference between these two systems in this respect is that the LBFS is significantly longer, and as is supported by the topographic analysis and seismic studies (Mortimer et al. 2007), consists of at least two major segments that have linked together to form a continuous escarpment. The analyzed segment of the UBFS on is similar in scale to one of the LBFS segments. The lack of a second knickpoint along the UBFS is consistent with the interpretation that the lowest, most recently developed knickpoint in the LBFS is a result of two large border fault segments similar in scale to the analyzed portion of the UBFS, linking together.

CHAPTER 6

CONCLUSION AND FUTURE WORK

The Malawi Rift is a unique laboratory where long continuous rift flanks intersect well-documented gradients in rainfall and rift basin characteristics. This grants a unique opportunity to study both the dynamics of large extensional faults and the impact these environmental parameters have on upland erosion in a well-controlled field study. Furthermore, the Livingstone and Usisya Rift flanks differ in their environmental gradients which allow for a robust comparison between the two systems and provides further opportunity to reveal any shortcomings in the assumptions. In both cases, the topography of these rift flanks appears to be consistent with theory that describes relationships between topography, tectonics, rainfall and baselevel controls. However, the resolution of the topographic datasets and lack of field observations limit the certainty of these findings.

Interpretations derived from the topography of the Livingstone and Usisya rift flanks provide insight into how these tectonic systems evolve over time. The topographic record indicates that the uplift rate along the entire rift flank is closely related to expansion and linking together of fault segments into a more continuous system. It is this behavior that creates well-graded channel reaches separated by knickpoints and enabling analysis of discrete intervals of rift-flank evolution. This correlation needs to be observed in other systems in order to more confidently distinguish between accelerated extension driving more rapid fault segment expansion and linkage vs. segment linking resulting in accelerated slip as extension is focused onto a dominant system.

Once rift flanks mature, they become important physiographic features capable of altering climate patterns within rift systems. In the case of the LBFS, an orographic precipitation gradient roughly correlates to topographic form in the lowermost reaches of channels, supporting the prediction that precipitation will affect the erosional efficiency of a system. Both the rainfall and topographic data are too coarse to quantitatively describe the observed relationship or determine whether spatially variable erosion controlled by precipitation patterns has any impact on tectonics.

In order to explore the dynamics of this system in more detail and further assess the validity of assumptions made in this analysis, field measurements of erosion rates need to be made. Strategic use of catchment averaged erosion rates along these rift systems can infer along-strike uplift patterns (Granger et al., 1996). In the event that there is a feedback between uplift and precipitation operating along these rift flanks, it is possible that higher uplift rates and more efficient erosion would have opposing effects on topography masking this feedback in the topographic analysis conducted here. Alternatively, erosion rate measurements could confirm the observation that dryer sections of the LBFS are associated with steeper channels if it is shown that uplift is not the cause of this steepening. Topographic analysis as presented in this thesis combined with the appropriate field techniques will be a valuable undertaking that will compliment basin studies to form a complete source-to-sink dataset capable of addressing some of the most elusive questions in landscape evolution.

CHAPTER 7

FIGURES

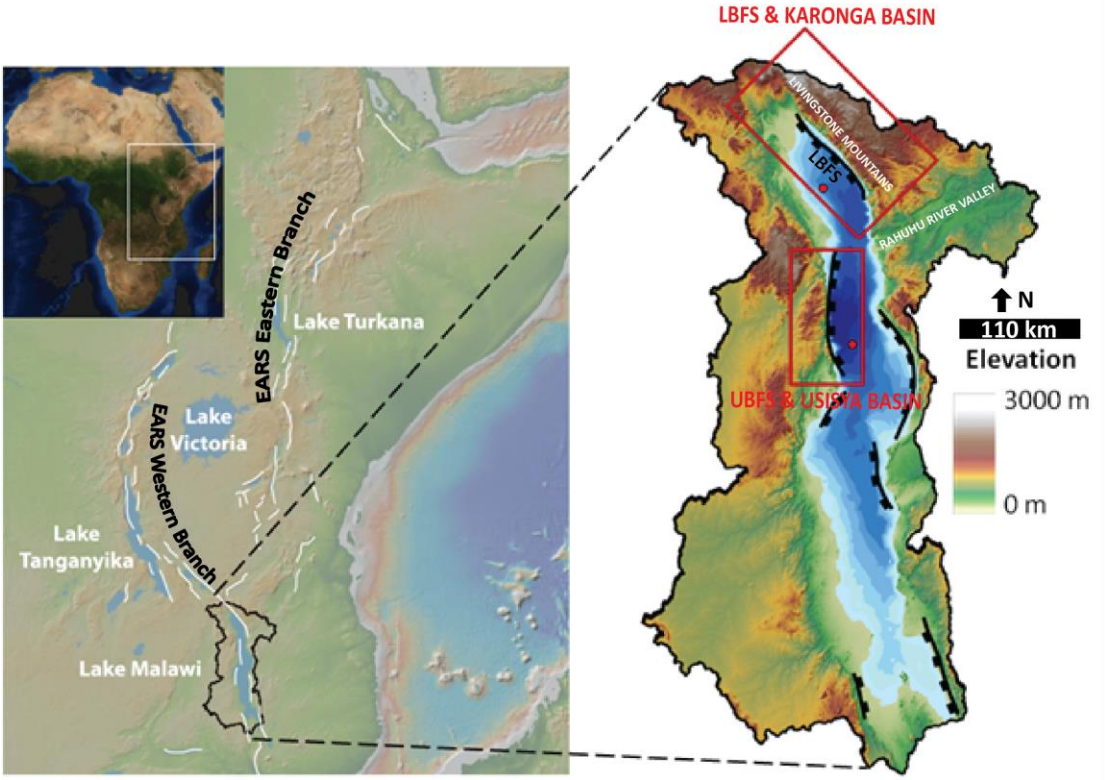

Figure 1 – Left: Regional map of the East African Rift System (EARS). White lines represent major border fault systems and major rift lakes are labeled. The EARS is split into an Eastern and a Western Branch and the Lake Malawi watershed is located at the southern end of the Western Branch. Right: Lake Malawi watershed showing elevation, bathymetry, location of border faults, location of scientific drill core locations (red dots). Red boxes outline the extent of future figures showing the study Livingstone Border Fault System (LBFS) and Usisya Border Fault System (UBFS) study areas.

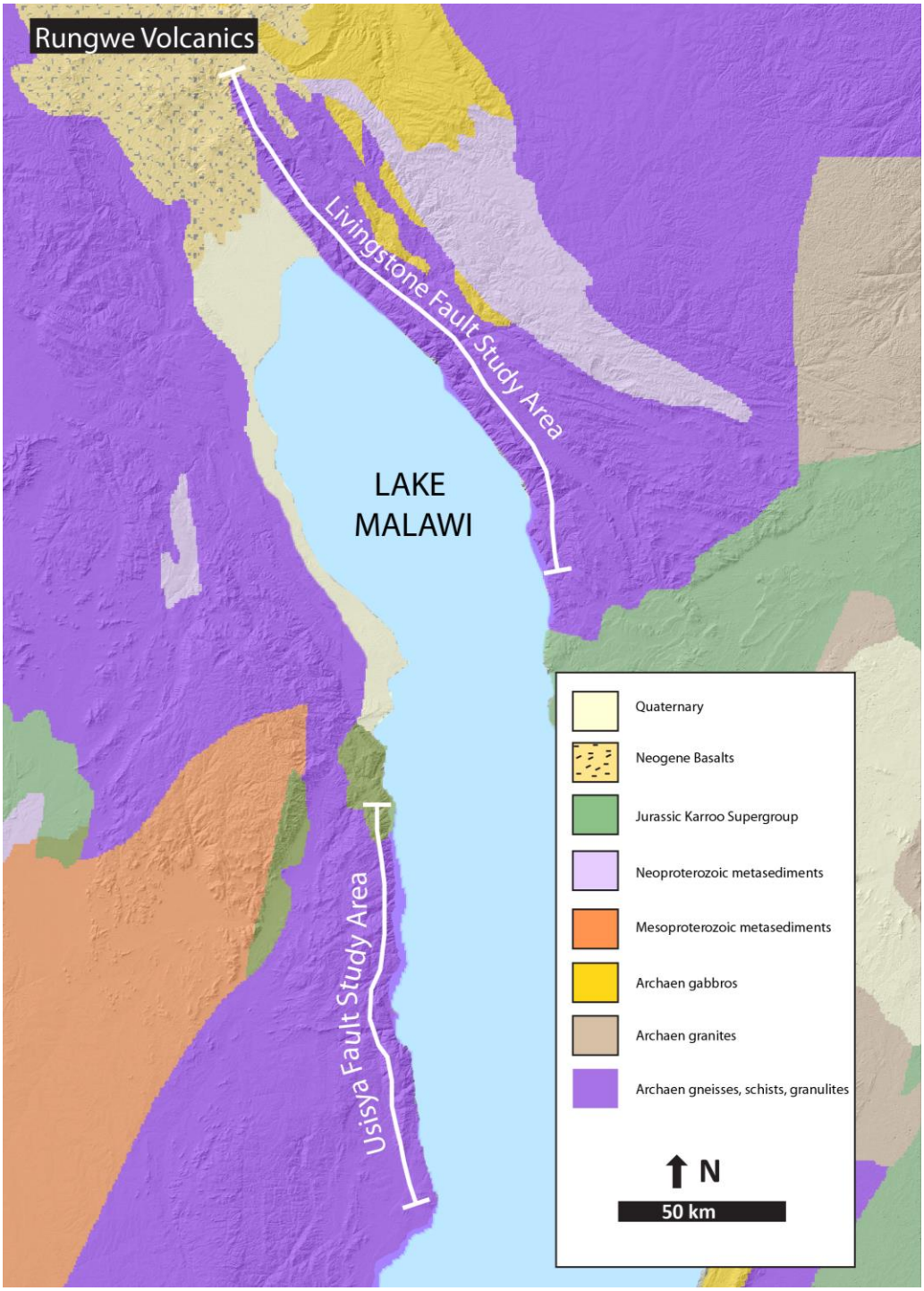

Figure 2 – Geologic map of the Lake Malawi region made with geomap (http://www.geomapapp.org, Ryan et al., 2009). The trace of the study areas are represented with white brackets. Both study areas are located predominantly in crystalline Archean rock types. Larger drainages from the study draining the Livingstone Border Fault System experience more lithologic diversity but rock types are still relatively hard.

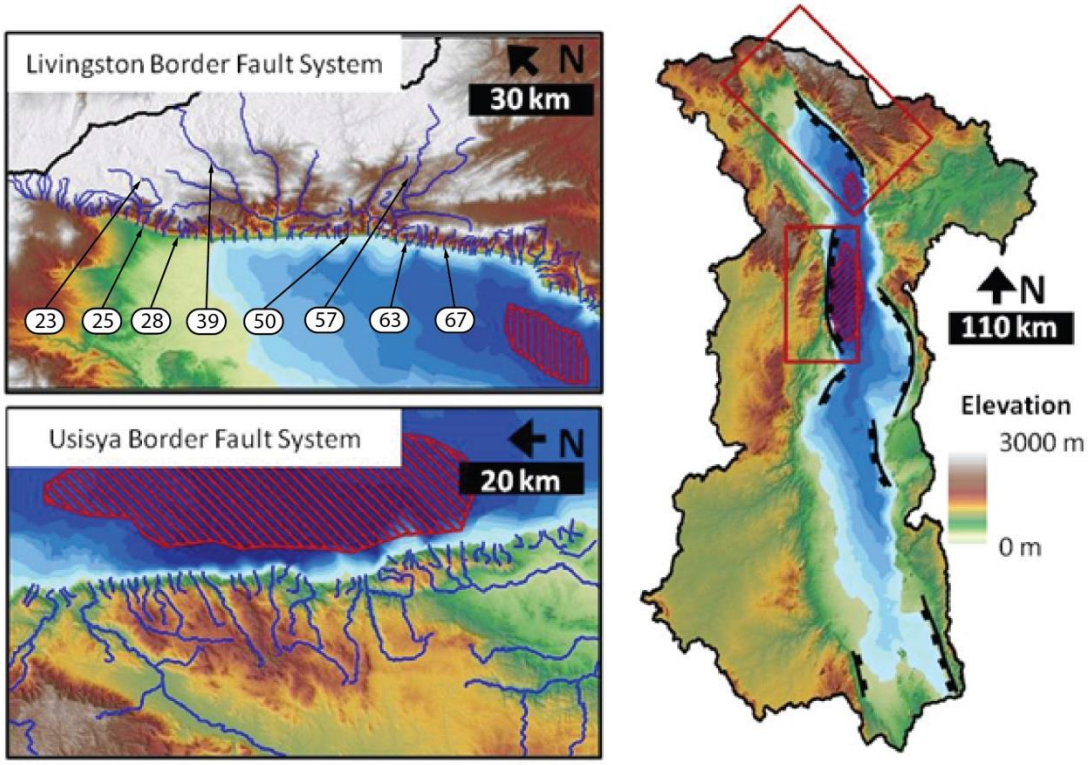

Figure 3 – Right: Lake Malawi watershed showing the extent of lake lowstands during Pleistocene dry periods (red hatches). Red squares denote extent of Livingstone Border Fault System and Usisya Border Fault System maps to the left. LEFT: Blue lines represent all drainages. Numbered drainages show the locations of longitudinal profiles (figures 7-14). Note that there is a clear distinction between short rangefront drainages and larger transverse drainages within the Livingstone Border Fault System. The larger drainages only flow into the Malawi basin at select places along the fault escarpment.

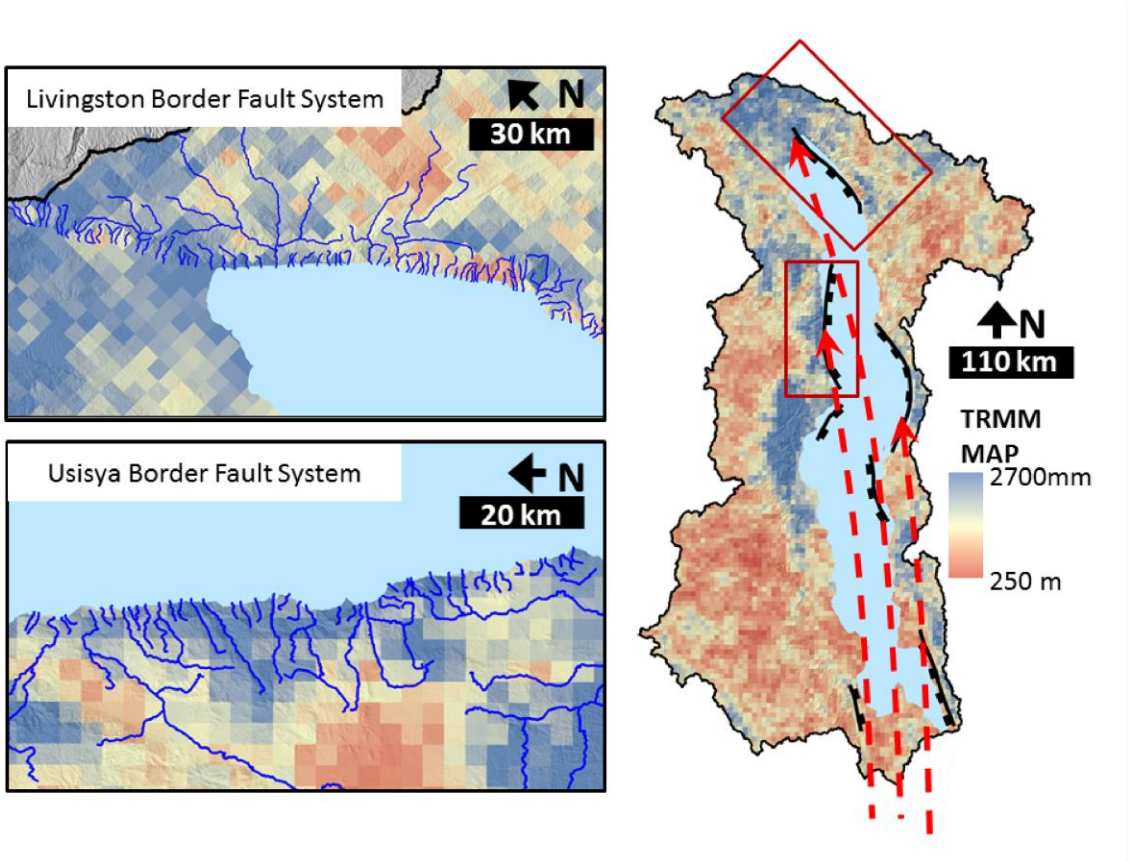

Figure 4 – Left: Lake Malawi watershed shows spatial heterogeneity in mean annual rainfall as quantified by the Tropical Rainfall Measuring Mission (TRMM) processed by Bookhagen et al. (in review) due to the interaction of high and or funneling topography and moist monsoonal weather pattern (red arrows). Right: Border fault escarpments show differing rainfall patterns. The Livingstone Border Fault System is characterized by a drying trend to the SE while the Usisya Border Fault System experiences more constant rainfall along the rangefront.

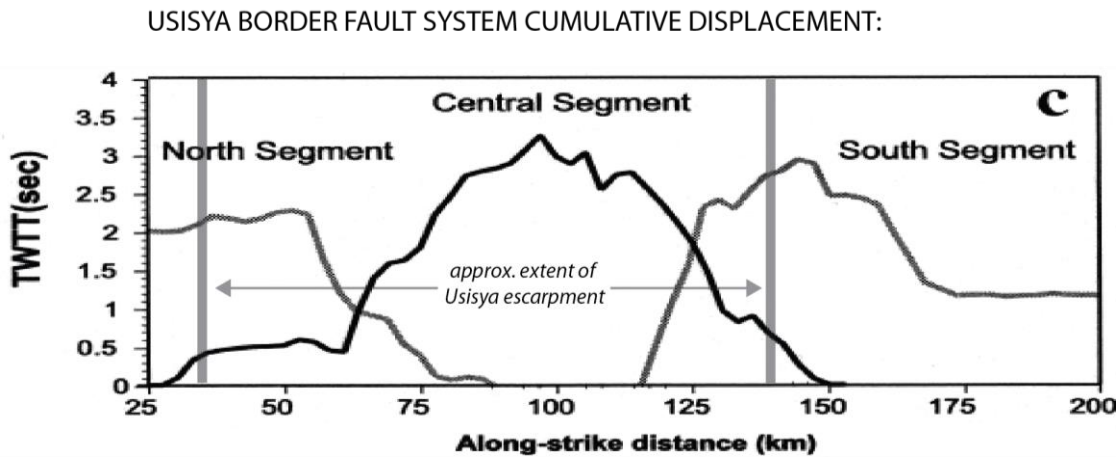

Figure 5 – Two way travel time (TWTT) depth to bedrock as interpreted by Contreras et al., 2000 for the Usisya Border Fault System. TWTT can act as a loose proxy for sediment thickness. The North and South segments are located off shore but the Central Segment produces the footwall relief within the Usisya Border Fault System study area. The Central Segment appears to have behaved like a restricted fault segment between 60-135 km along-strike but the tips, particularly the northern one, appear to be consistent with unrestricted fault growth. *Modified from Contreras et al. (2000).*

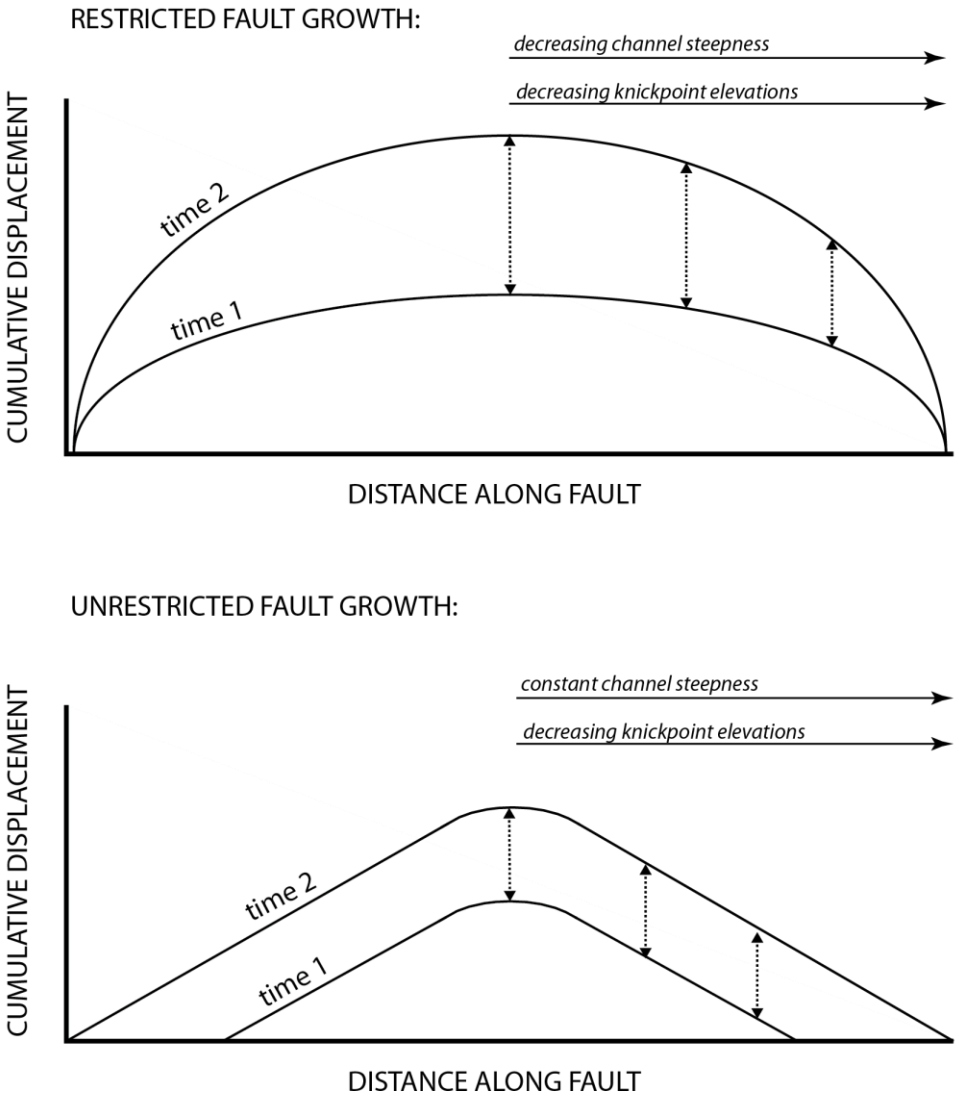

Figure 6 – Isochron lines represent total along-strike displacement at two hypothetical time steps for two different types of fault segments. Top: A fault with restricted growth at the fault tips requires displacement between time 1 and time 2 to go to zero meaning there will be a gradient in uplift rate, channel steepness, and knickpoint elevation (assuming contemporaneous knickpoints along-strike) towards the tips. This is represented by the decreased distance between time 1 and time 2 with the dashed lines. Bottom: If a fault segment is not restricted at the tips, it can grow proportional to its cumulative displacement, meaning no gradient in uplift rate, channel steepness or elevation of any contemporaneous knickpoints. Knickpoint elevations in this model will decrease if they are associated with the fault growth and not contemporaneous. These are two idealized models and real systems will likely behave like a hybrid of these two models in space and time. *Modified from Manighetti et al. 2001.*

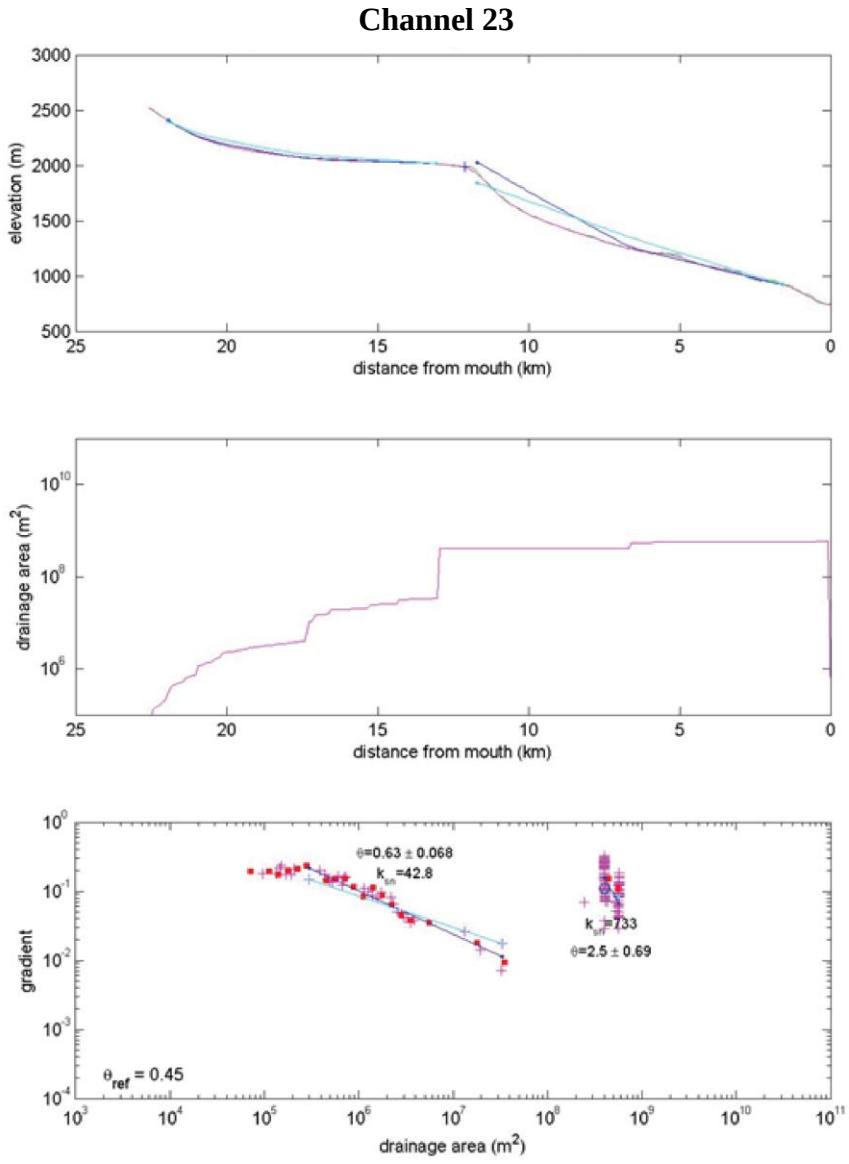

Figure 7 – Longitudinal profile information for channel 23 (transverse drainage) from the Livingstone Border Fault System. See figure 3 for location information. Top: Longitudinal profile shows a discrete knickpoint separating two fairly well-adjusted reaches of channel with a subtle convexity visible near the outlet. Middle: Drainage area plotted against channel length to ensure that measurements are not influence by confluences with large tributaries. Bottom: Slope-area plot shows that the lower reach is described by a higher channel steepness (y-intercept of regressions) indicating that the drainage has experienced an increase in uplift rate or decrease in erosional efficiency.

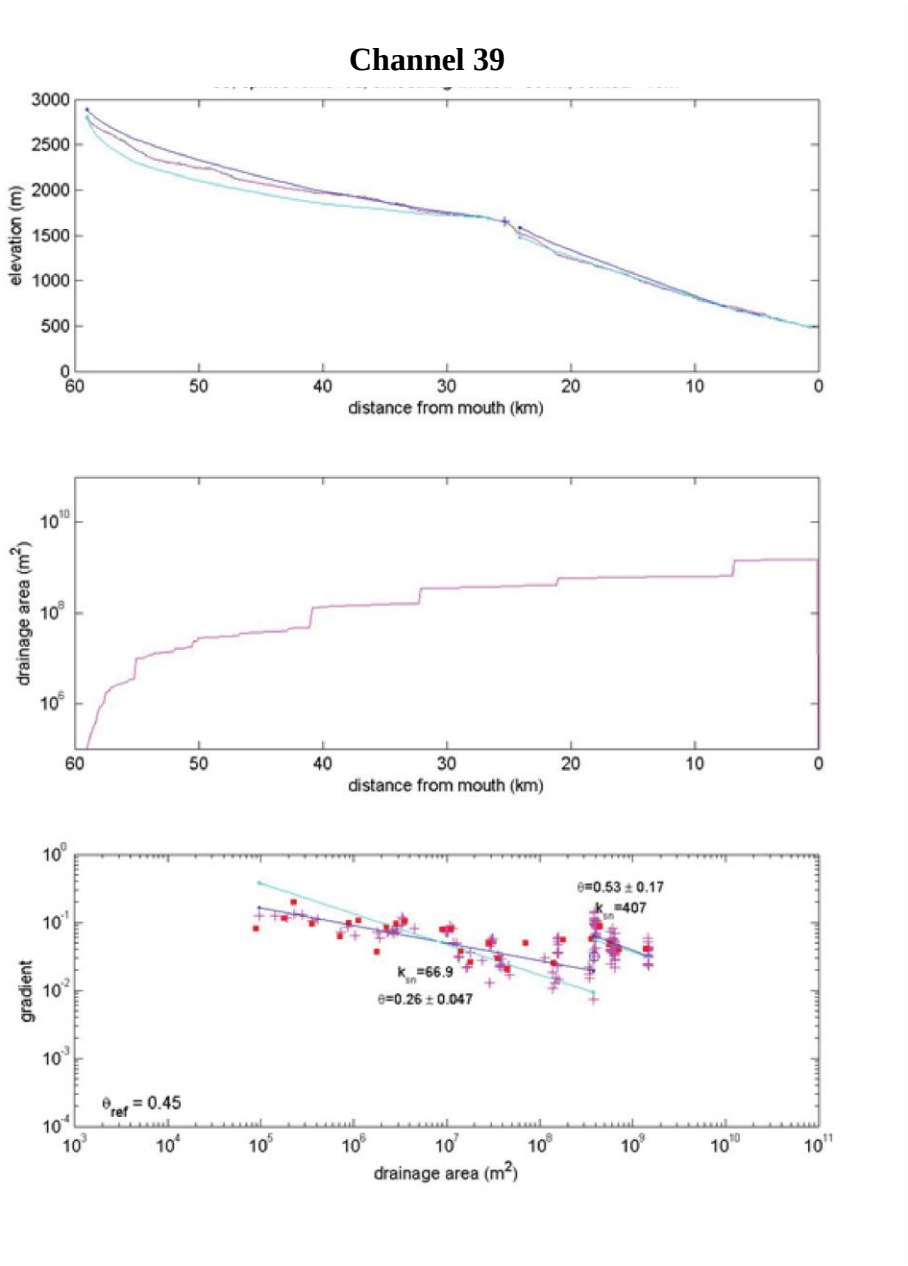

Figure 8 – Longitudinal profile information for channel 39 (transverse drainage) from the Livingstone Border Fault System. See figure 3 for location information. Top: Longitudinal profile shows a discrete knickpoint separating two fairly well-adjusted reaches of channel. Middle: Drainage area plotted against channel length to ensure that measurements are not influence by confluences with large tributaries. Bottom: Slope-area plot shows that the lower reach is described by a higher channel steepness (y-intercept of regressions) indicating that the drainage has experienced an increase in uplift rate or decrease in erosional efficiency.

Channel 57

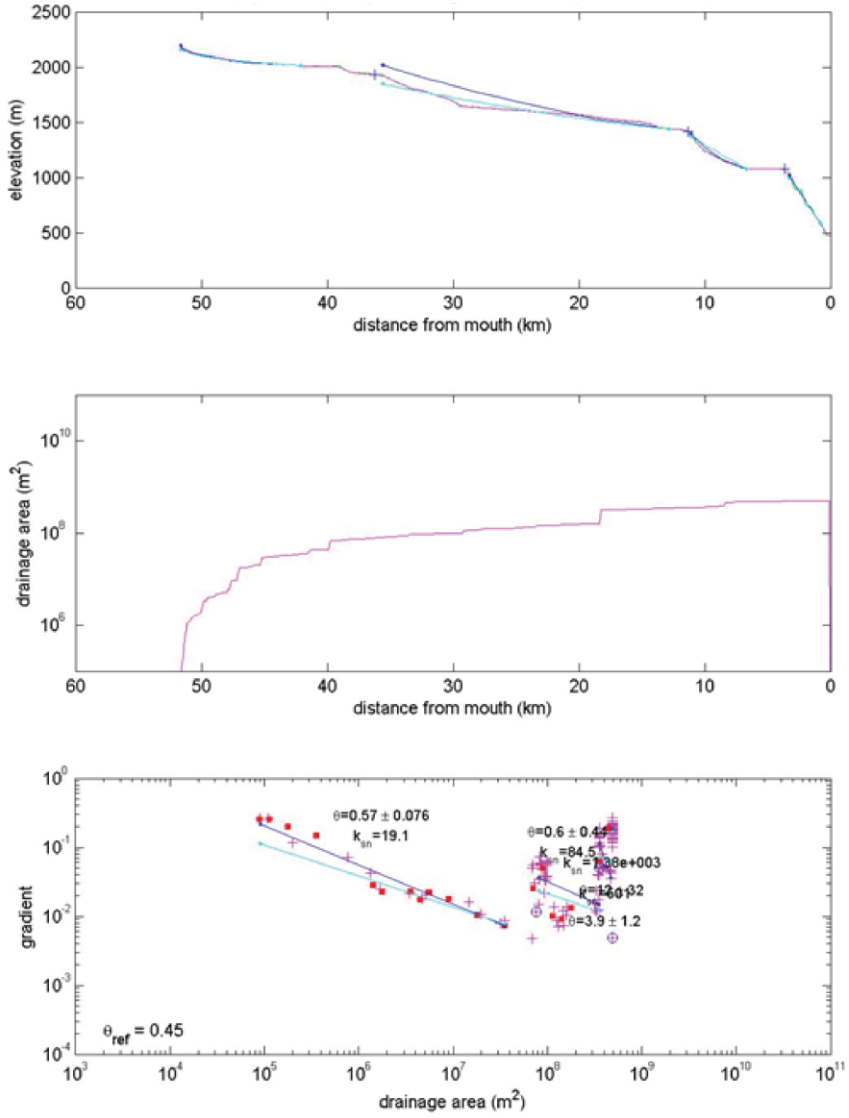

Figure 9 – Longitudinal profile information for channel 57 (transverse drainage) from the Livingstone Border Fault System. See figure 3 for location information. Top: Longitudinal profile shows 3 clearly defined knickpoints separating four channel reaches Middle: Drainage area plotted against channel length to ensure that measurements are not influence by confluences with large tributaries. Bottom: Slope-area plot shows that the lower reaches are described by progressively higher channel steepness (y-intercept of regressions). Given consistency with channel 23 and 39 it is likely that one of these knickpoints is correlative with the major knickpoints in the other channels. The presence of the other knickpoints suggests complications unique to this transverse drainage.

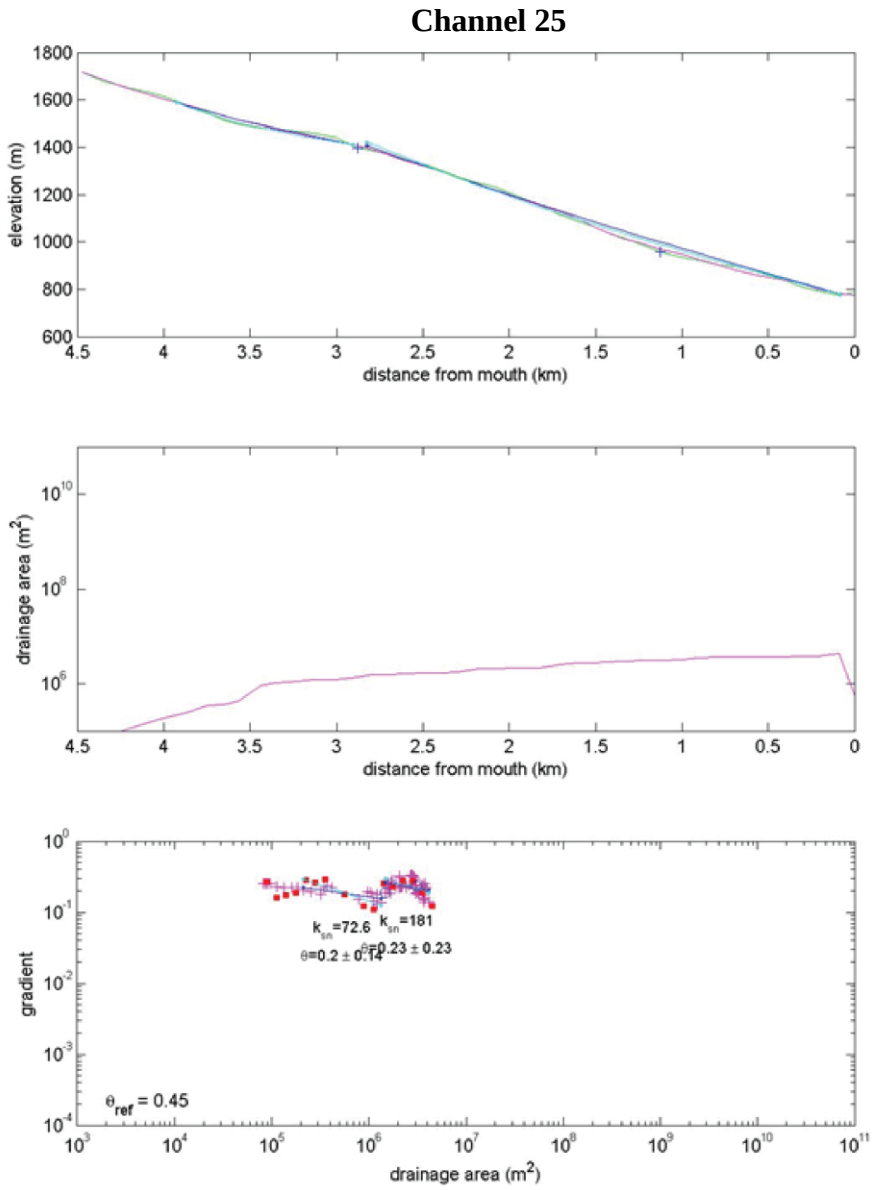

Figure 10 – Longitudinal profile information for channel 25 (rangefront drainage) from the Livingstone Border Fault System. See figure 3 for location information. Top: Longitudinal profile shows a knickpoint separating two fairly well-adjusted reaches of channel. Middle: Drainage area plotted against channel length to ensure that measurements are not influence by confluences with large tributaries. Bottom: Slope-area plot more clearly shows the knickpoint with higher steepness measured in the lower reach (consistent with transverse drainages).

Channel 28

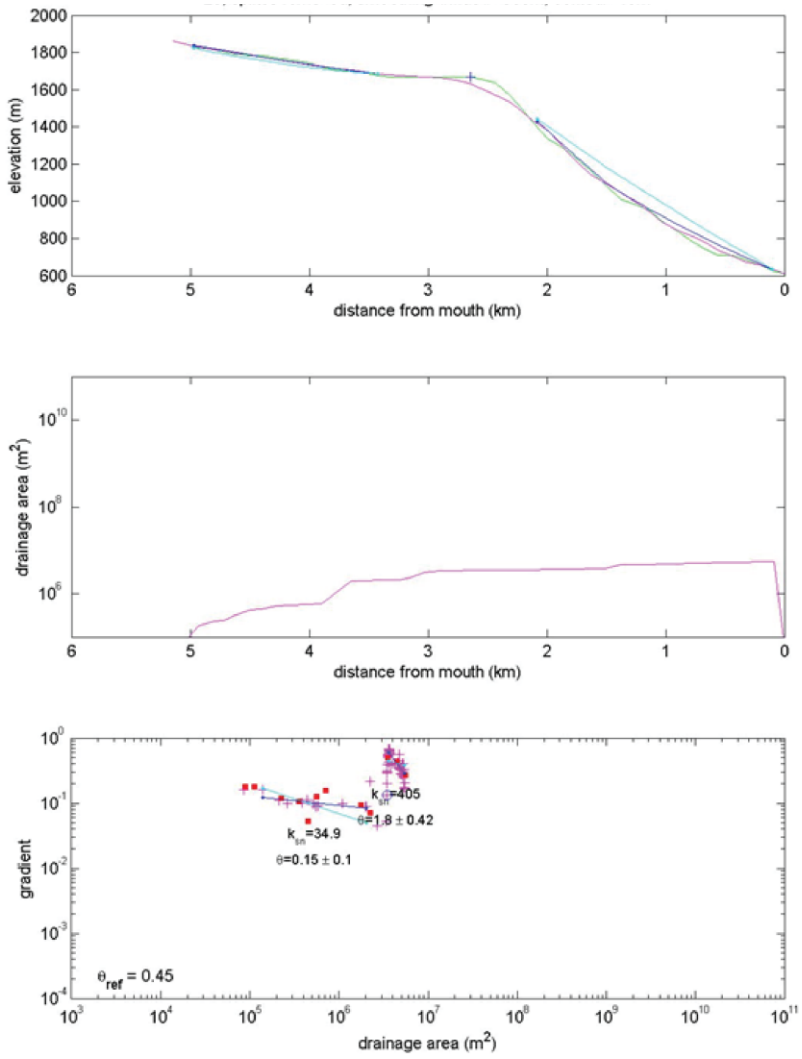

Figure 11 – Longitudinal profile information for channel 28 (rangefront drainage) from the Livingstone Border Fault System. See figure 3 for location information. Top: Longitudinal profile shows a knickpoint separating two well-adjusted reaches of channel. Note that upper reach is sizable and exceptionally low in relief. Middle: Drainage area plotted against channel length to ensure that measurements are not influence by confluences with large tributaries. Bottom: Slope-area plot more clearly shows the knickpoint with extremely high steepness values below the knickpoint (405). While the pattern of steepening is consistent with channel 23, it is unlikely that the two knickpoint are correlative. Small rangefront drainages that capture large areas of high elevation and low relief terrain are the source of many outliers in this study, likely due to a lack of sediment being supplied from these upper reaches.

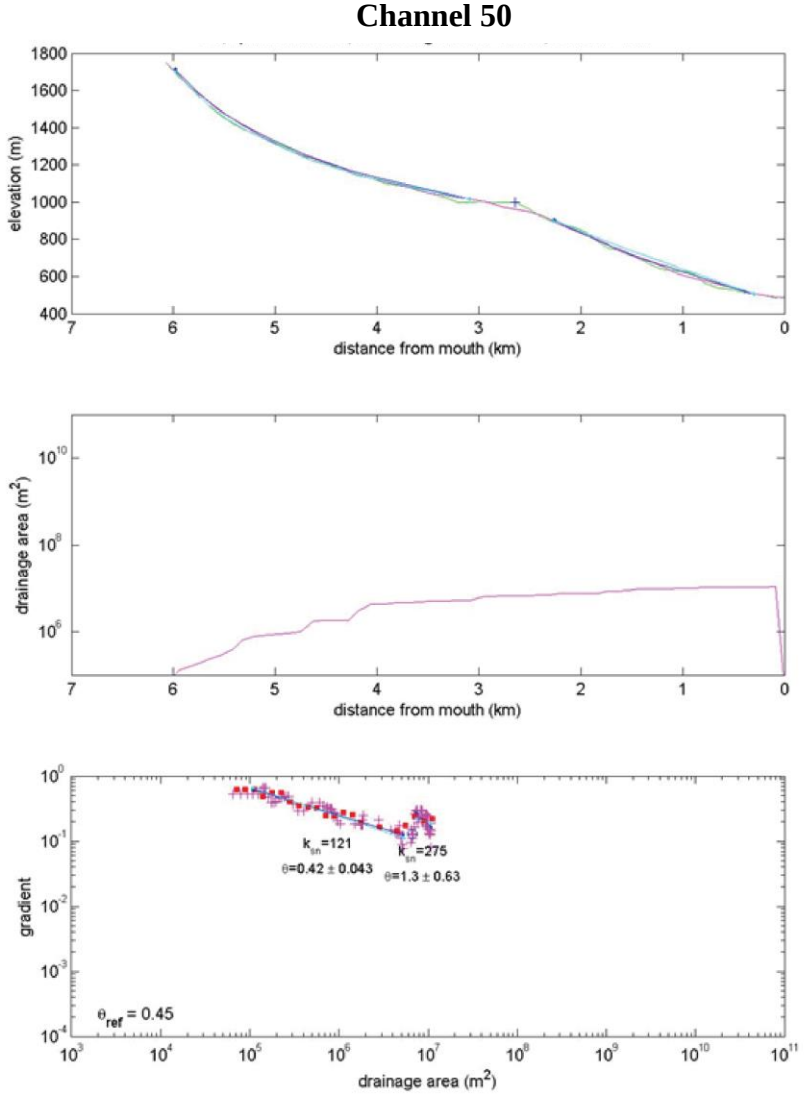

Figure 12 – Longitudinal profile information for channel 50 (rangefront drainage) from the Livingstone Border Fault System. See figure 3 for location information. Top: Longitudinal profile shows a knickpoint separating two well-adjusted reaches of channel. Note the elevation of the knickpoint has decreased relative to channel 25. Middle: Drainage area plotted against channel length to ensure that measurements are not influence by confluences with large tributaries. Bottom: The lower reach continues to be described by higher steepness values. Note that the channel steepness of the lower reach is not significantly higher than channel 23 (which was similar in form). This is representative of this section of the fault and corresponds to lower MAP along the rangefront.

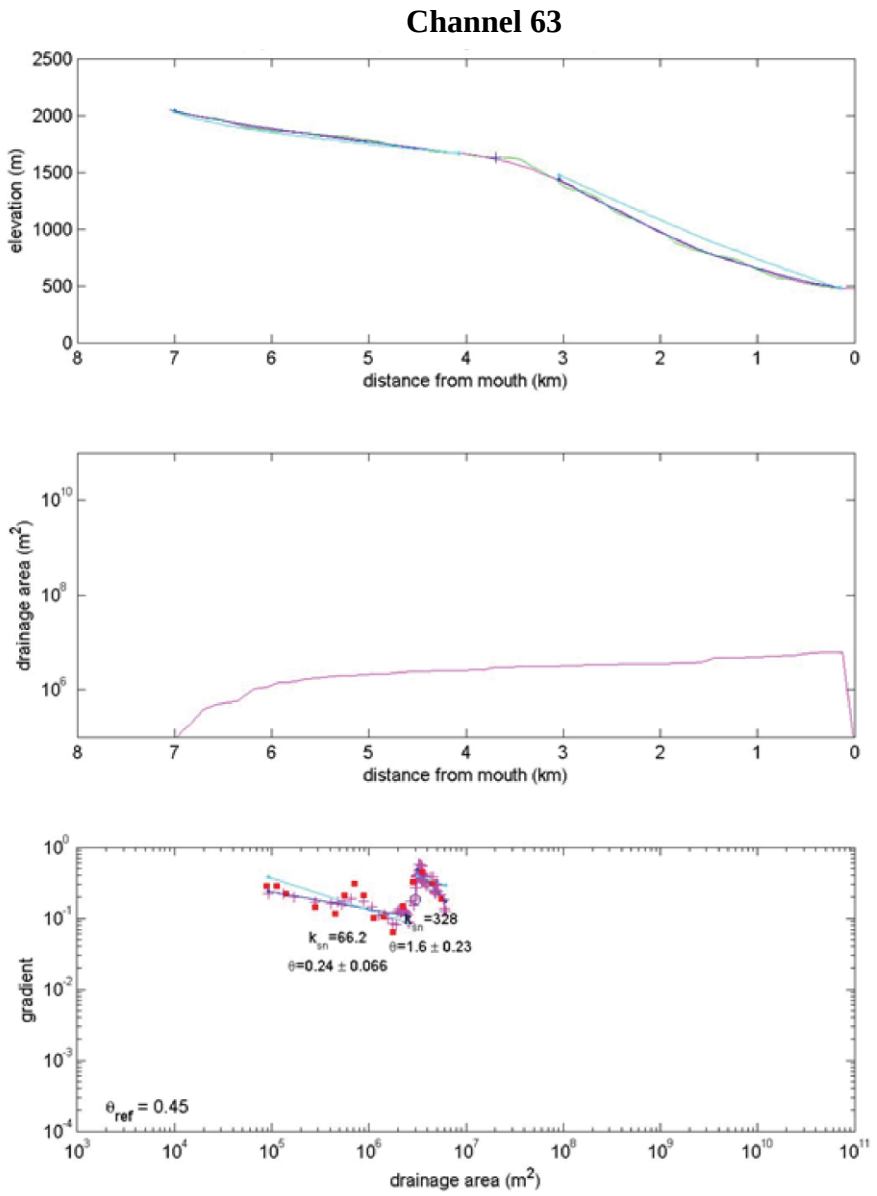

Figure 13 – Longitudinal Longitudinal profile information for channel 63 (rangefront drainage) from the Livingstone Border Fault System. See figure 3 & 15 for location information. Top: Longitudinal profile shows another knickpoint separating two well-adjusted reaches of channel. Middle: Drainage area plotted against channel length to ensure that measurements are not influence by confluences with large tributaries. Bottom: This channel is located along the driest portion of the Livingstone Border Fault System and is characterized by one of the highest channel steepness values in the lower reach.

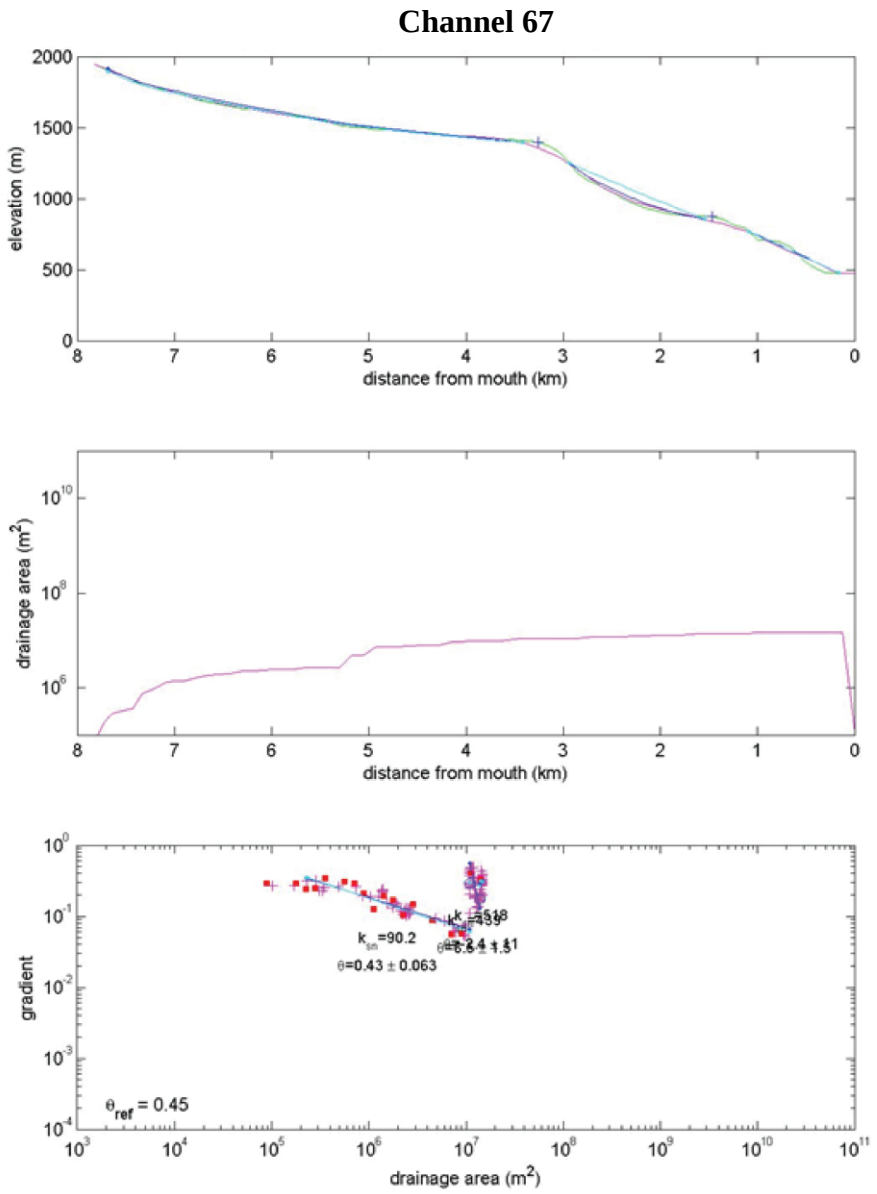

Figure 14 – Longitudinal profile information for channel 67 (rangefront drainage) from the Livingstone Border Fault System. See figure 3 & 15 for location information. Top: Longitudinal profile shows two knickpoints separating three reaches of channel. Middle: Drainage area plotted against channel length to ensure that measurements are not influence by confluences with large tributaries. Bottom: This channel is located along the driest portion of the Livingstone Border Fault System but high channel steepness value (>500) in the lowest reach appears to be a result of an extra knickpoint identified that is not contemporaneous others along-strike.

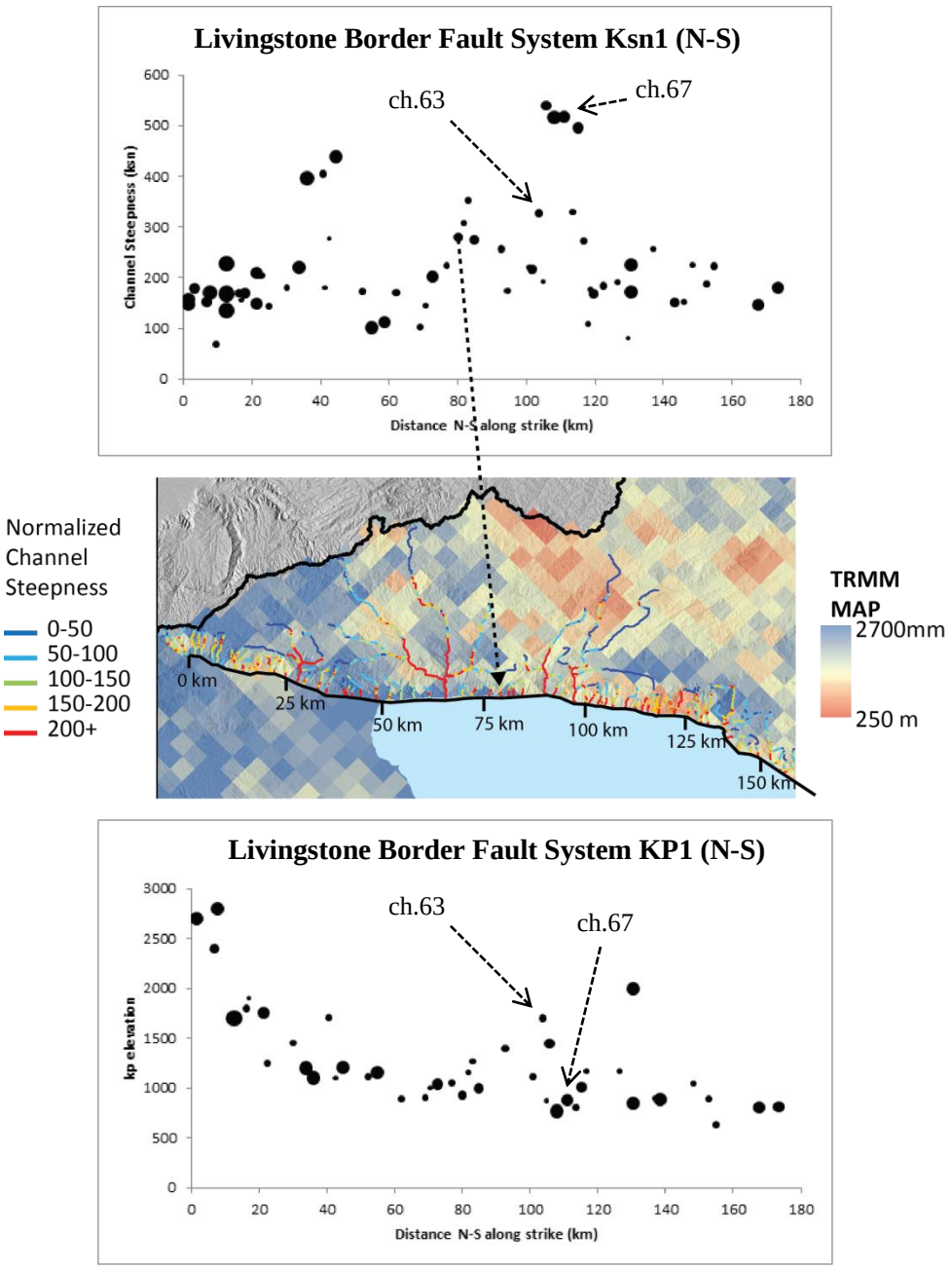

Figure 15 – Top: Along-strike values of Ksn1 for the Livingstone Border Fault System show increase along the central portion of the fault. Middle: The increase in Ksn1 occurs over the same distance that MAP decreases (see figure 21 for plotted along strike values). Bottom: KP1 elevation decreases quickly from the NW edge of the study area before stabilizing at ~1000 m. The size of data points corresponds to drainage area, which ranges between 4-25 km^2

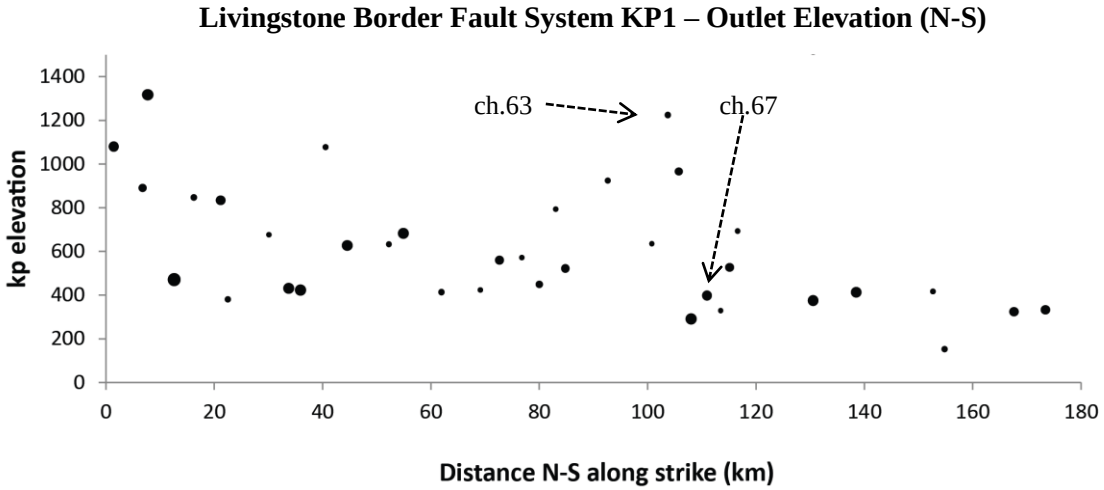

Figure 16 – Outlet elevations where rangefront channels crossed the fault trace were subtracted from knickpoint elevations in order to remove the effect of variable baselevel within the study area. The size of data points corresponds to drainage area, which ranges between 4-25 km^2.

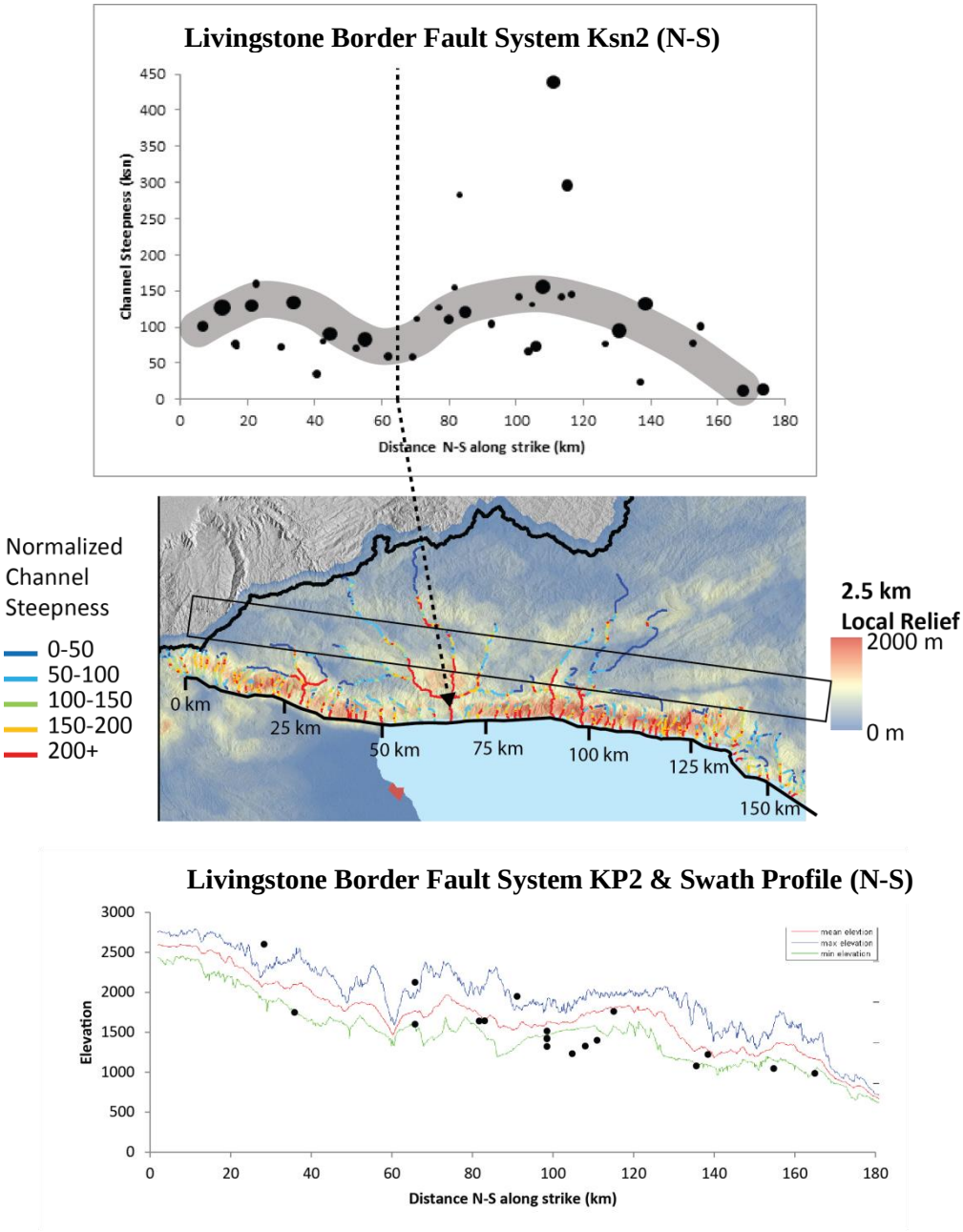

Figure 17 – Top: Two semi-elliptical Ksn2 patterns support the interpretation that the Livingstone Border Fault System was composed of two independent fault systems that linked together. Size of data points corresponds to drainage area, which ranges between 4-25 km^2. Middle: The low in Ksn2 values from the top panel corresponds to the location of the central transverse drainage, also consistent with notion of two independent faults with a thru-flowing channel running between them. The black rectangle represents the extent of the 10km swath in the bottom panel. Bottom: The elevation of KP2 (on all channel sizes) correlates with the high-elevation low-relief erosional surface behind the Livingstone Escarpment.

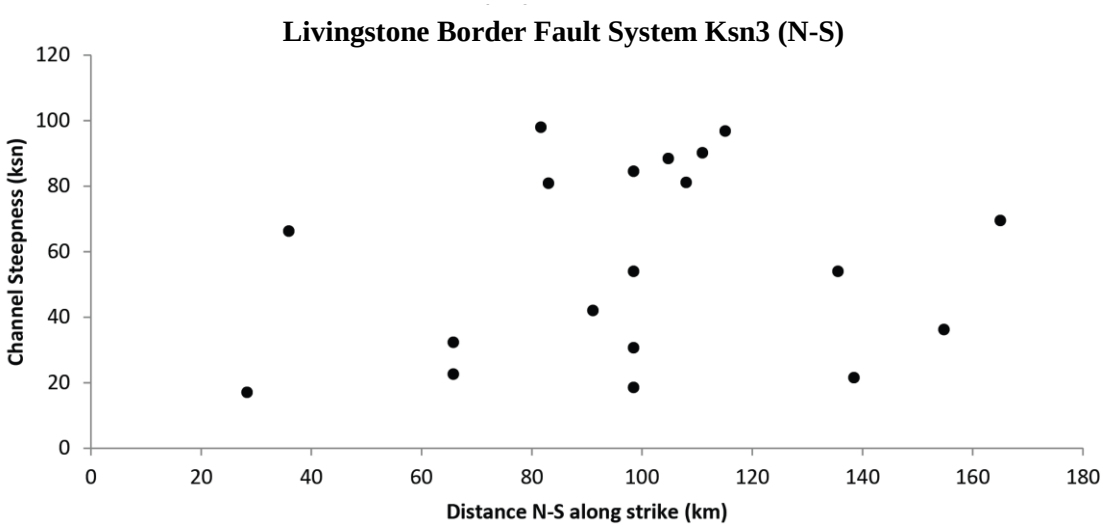

Figure 18 – Above KP2, channel reaches are characterized by low gradients and no along-strike pattern. This supports the interpretation that KP2 and Ksn3 are recording early stages of rifting where pale relief and small distributed faults shape the topography.

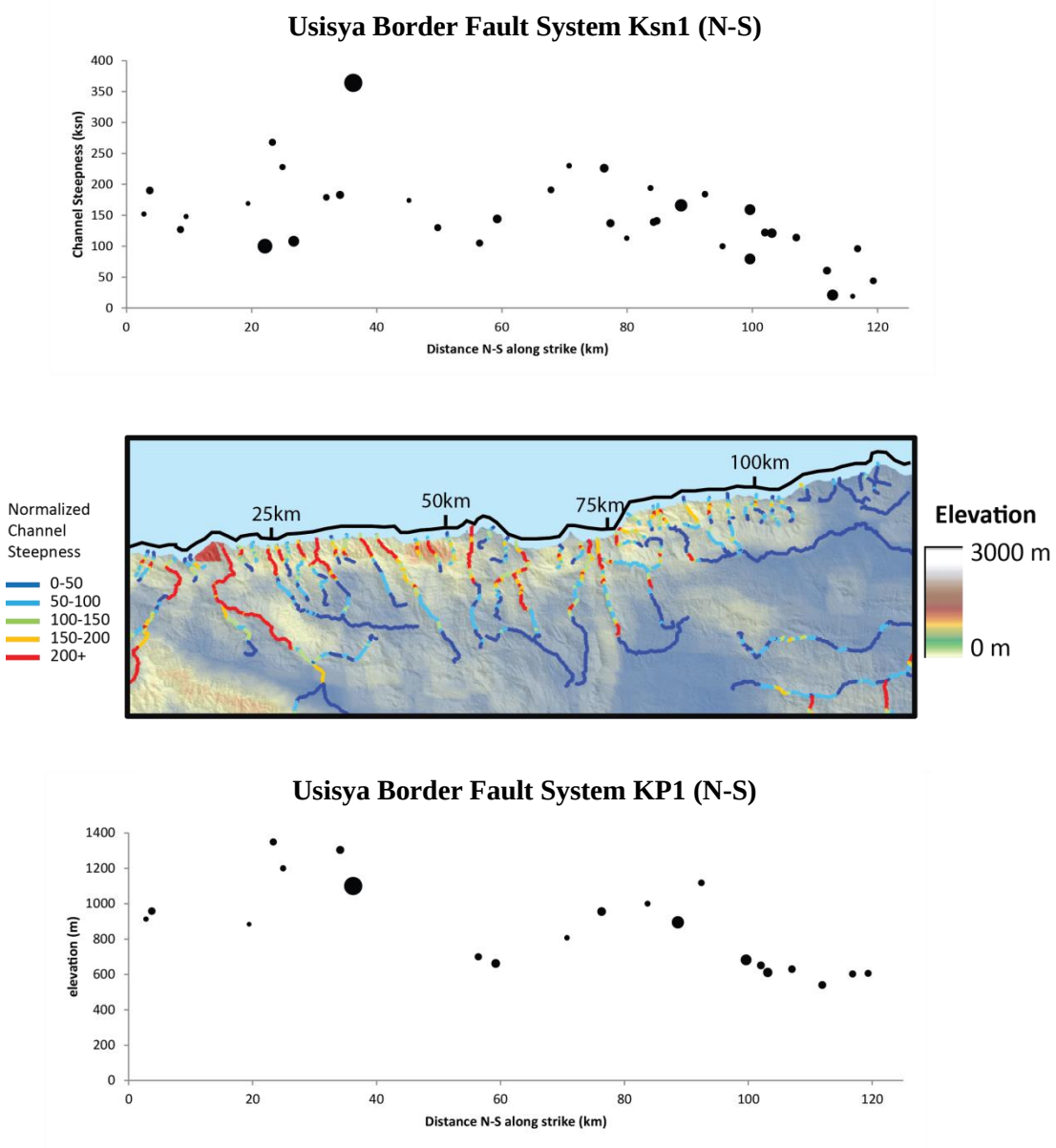

Figure 19 – Top: Steady Ksn1 value until ~90 km and decreasing values thereafter suggest that this fault tip is behaving as if it is restricted on one end. Middle: A 2.5 km radius relief map mirrors the Ksn1 pattern. Bottom: knickpoint elevations also show a decrease along the southern tip of the fault. The size of data points corresponds to drainage area, which ranges between 2.5-40 km^2.

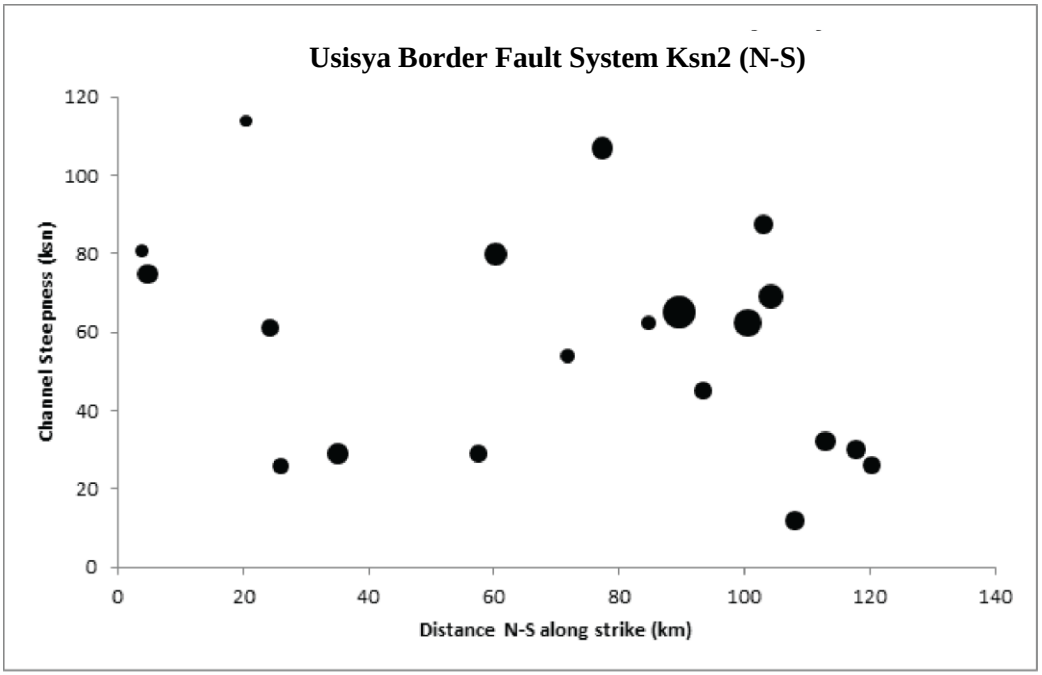

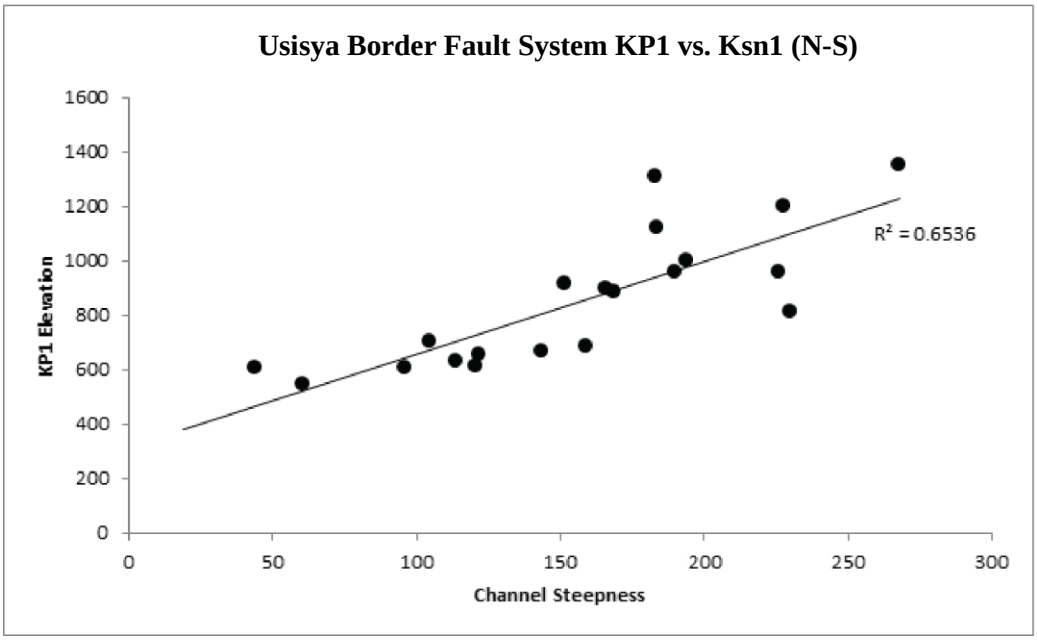

Figure 20 – Top: The low and variable values of Ksn2 here are analogous to Ksn3 from the Livingstone Border Fault System and likely represent paleotopography and early rifting. The size of data points corresponds to drainage area, which ranges between 2.5-40 km^2. Bottom: Ksn1 and Kp1 elevation are positively correlated, following the expected relationship for a restricted growth fault (figure 6).

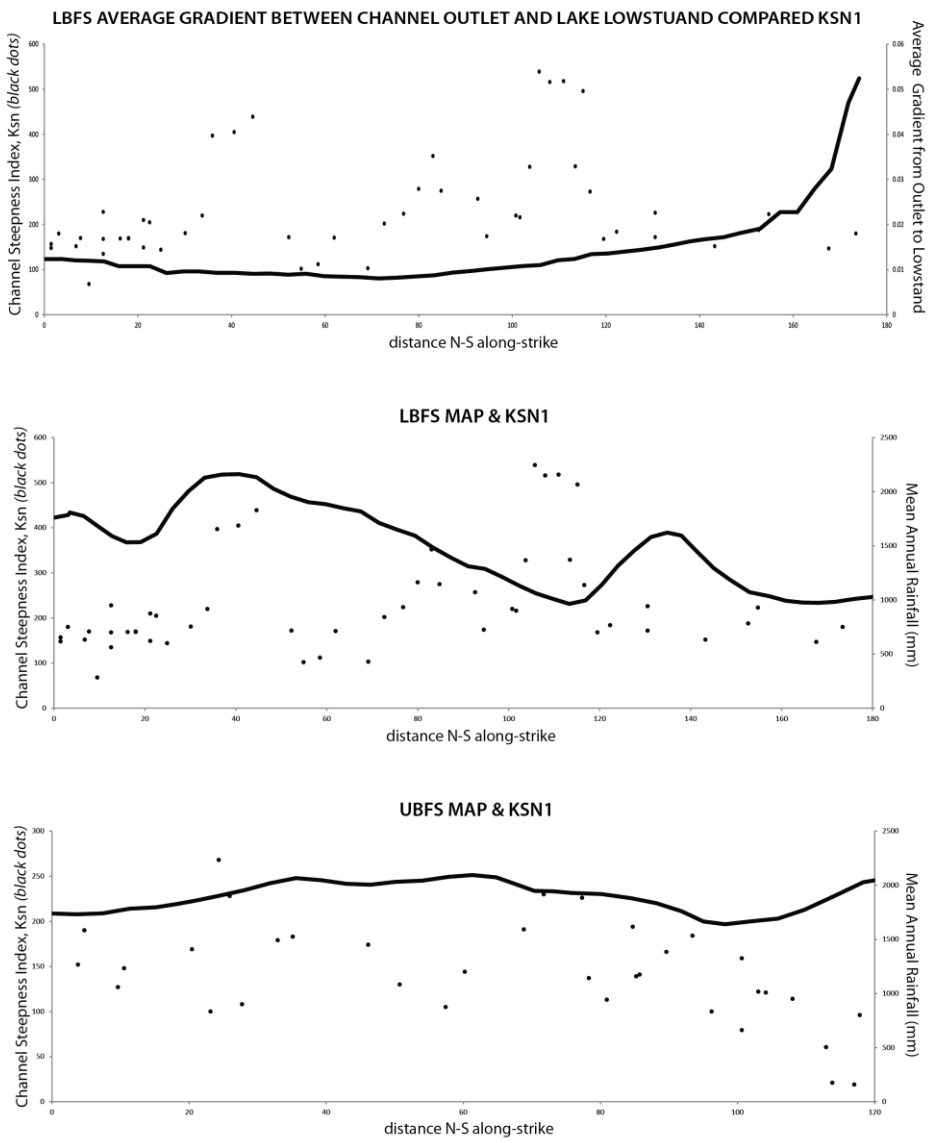

Figure 21 – Comparison of Livingstone Border Fault System Ksn1 to different environmental parameters. Top: average gradient between channel outlet and lake low stand (black line) increases dramatically from 140-180 km along-strike with no increase in Ksn1, as would be expected if lake level fluctuation was driving incision. Middle: along-strike rainfall (averaged over 20-km window) within 8km of the shoreline (black line) shows that increased Ksn1 values between 60-120 km along strike are crudely mirrored by decreases in MAP along the Livingstone Border Fault System. This observation is consistent with the interpretation that climate has measurably impacted denudation since the development of an orographic rainfall gradient. Lower: The Usisya Border Fault System experiences more constant rainfall (measured using the same methodology) than the Livingstone Border Fault System and therefore exhibits no climate induced channel steepening.

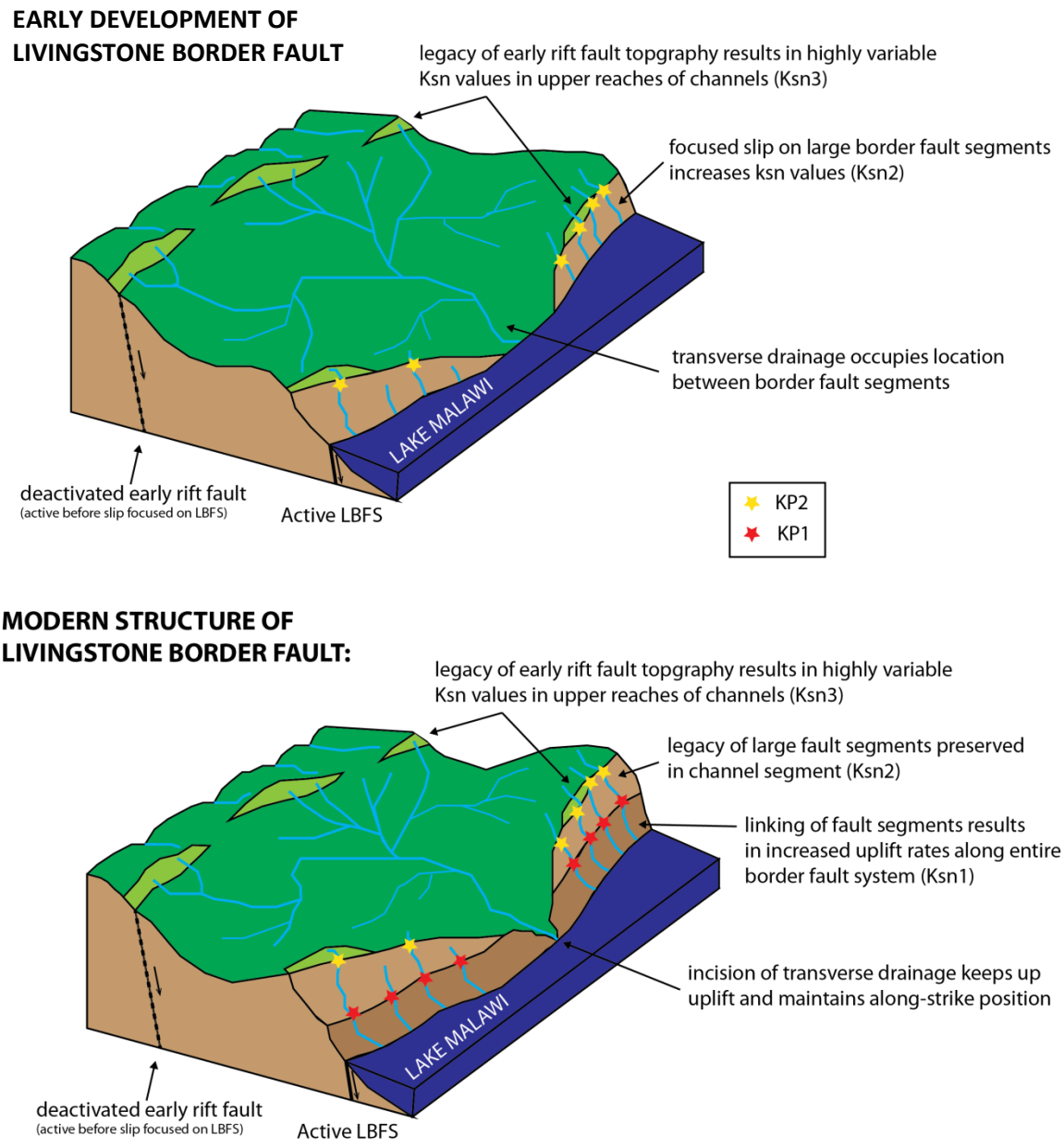

Figure 22 – Conceptual cartoon of two major stages in rift development as observed along the Livingstone Border Fault System. Top: As early dispersed rifting matures and faults link up, large border fault systems develop and cannibalize slip from smaller faults. This creates a knickpoint between the early rift relief and the relief generated by these more mature structures (KP2- yellow star). These larger fault systems will diver drainages around them and river systems will occupy topographic lows between faults. Bottom: When two larger border faults link together, the transition from restricted growth to unrestricted growth and footwall uplift accelerates along the entire system creating another knickpoint that begins to move through the system (KP1 – red star). The drainage systems that previously flow between fault segments become entrenched in their location. *Modified from Cowie et al. 2005.*

REFERENCES

Beuning, K. R. M., K. A. Zimmerman, et al. (2011). "Vegetation response to glacial-interglacial climate variability near Lake Malawi in the southern African tropics." Palaeogeography Palaeoclimatology Palaeoecology 303(1-4): 81-92.

Biggs, J., E. Nissen, et al. (2010). "Breaking up the hanging wall of a rift-border fault: The 2009 Karonga earthquakes, Malawi." Geophysical Research Letters 37.

Bookhagen, B. (in review): High resolution spatiotemporal distribution of rainfall seasonality and extreme events based on a 12-year TRMM time series, in review.

Brown, E. T., T. C. Johnson, et al. (2007). "Abrupt change in tropical African climate linked to the bipolar seesaw over the past 55,000 years." Geophysical Research Letters 34(20).

Cartwright, J., B. Trudgill, et al. (2000). "Fault growth by segment linkage: an explanation for scatter in maximum displacement and trace length data from the Canyonlands grabens of SE Utah: Reply." Journal of Structural Geology 22(1): 141-143.

Cartwright, J. A., B. D. Trudgill, et al. (1995). "Fault Growth by Segment Linkage - an Explanation for Scatter in Maximum Displacement and Trace Length Data from the Canyonlands Grabens of Se Utah." Journal of Structural Geology 17(9): 1319-1326.

Chorowicz, J. (2005). "The East African rift system." Journal of African Earth Sciences 43(1-3): 379-410.

Cohen, A. S., J. R. Stone, et al. (2007). "Ecological consequences of early Late Pleistocene megadroughts in tropical Africa." Proceedings of the National Academy of Sciences of the United States of America 104(42): 16422-16427.

Contreras, J., M. H. Anders, et al. (2000). "Growth of a normal fault system: observations from the Lake Malawi basin of the east African rift." Journal of Structural Geology 22(2): 159-168.

Cowie, P. A., J. R. Underhill, et al. (2005). "Spatio-temporal evolution of strain accumulation derived from multi-scale observations of Late Jurassic rifting in the northern North Sea: A critical test of models for lithospheric extension." Earth and Planetary Science Letters 234(3-4): 401-419.

Davis, K., D. W. Burbank, et al. (2005). "Thrust-fault growth and segment linkage in the active Ostler fault zone, New Zealand." Journal of Structural Geology 27(8): 1528-1546.

Dawers, N. H. and J. R. Underhill (2000). "The role of fault interaction and linkage in controlling synrift stratigraphic sequences: Late Jurassic, Statfjord East area, northern North Sea." Aapg Bulletin-American Association of Petroleum Geologists 84(1): 45-64.

DiBiase, R. A., K. X. Whipple, et al. (2010). "Landscape form and millennial erosion rates in the San Gabriel Mountains, CA." Earth and Planetary Science Letters 289(1-2): 134-144.

Ebinger, C. J., A. L. Deino, et al. (1989). "Chronology of Volcanism and Rift Basin Propagation - Rungwe Volcanic Province, East-Africa." Journal of Geophysical Research-Solid Earth and Planets 94(B11): 15785-&.

Ebinger, C. J., A. L. Deino, et al. (1993). "Tectonic Controls on Rift Basin Morphology - Evolution of the Northern Malawi (Nyasa) Rift." Journal of Geophysical Research-Solid Earth 98(B10): 17821-17836.

Ebinger, C. J., J. A. Jackson, et al. (1999). "Extensional basin geometry and the elastic lithosphere." Philosophical Transactions of the Royal Society of London Series a-Mathematical Physical and Engineering Sciences 357(1753): 741-762.

Ebinger, C. J., B. R. Rosendahl, et al. (1987). "Tectonic Model of the Malawi Rift, Africa." Tectonophysics 141(1-3): 215-235.

Flannery, J. W. and B. R. Rosendahl (1990). "The Seismic Stratigraphy of Lake Malawi, Africa - Implications for Interpreting Geological Processes in Lacustrine Rifts." Journal of African Earth Sciences 10(3): 519-548.

Flint, J. J. (1974). "Stream Gradient as a Function of Order, Magnitude, and Discharge." Water Resources Research 10(5): 969-973.

Granger, D. E., J. W. Kirchner, et al. (1996). "Spatially averaged long-term erosion rates measured from in situ-produced cosmogenic nuclides in alluvial sediment." Journal of Geology 104(3): 249-257.

Howard, A. D. and G. Kerby (1983). "Channel Changes in Badlands." Geological Society of America Bulletin 94(6): 739-752.

Johnson, T. C., E. T. Brown, et al. (2002). "A high-resolution paleoclimate record spanning the past 25,000 years in southern East Africa." Science 296(5565): 113-+.

King (1955). "Pediplanation and Isostasy: An example from South Africa." Quarterly Journal of the Geological Society(111): 353-359.

Lyons, R. P., C. A. Scholz, et al. (2011). "Late Quaternary stratigraphic analysis of the Lake Malawi Rift, East Africa: An integration of drill-core and seismic-reflection data." Palaeogeography Palaeoclimatology Palaeoecology 303(1-4): 20-37.

Manighetti, I., G. C. P. King, et al. (2001). "Slip accumulation and lateral propagation of active normal faults in Afar." Journal of Geophysical Research-Solid Earth 106(B7): 13667-13696.

Mortimer, E., D. A. Paton, et al. (2007). "Orthogonal to oblique rifting: effect of rift basin orientation in the evolution of the North basin, Malawi Rift, East Africa." Basin Research 19(3): 393-407.

Ring, U., C. Betzler, et al. (1992). "Normal Vs Strike-Slip Faulting during Rift Development in East-Africa - the Malawi Rift." Geology 20(11): 1015-1018.

Rosendahl, B. R., E. Kilembe, et al. (1992). "Comparison of the Tanganyika, Malawi, Rukwa and Turkana Rift Zones from Analyses of Seismic-Reflection Data." Tectonophysics 213(1-2): 235-256.

Scholz, C. A. (1995). "Deltas of the Lake Malawi Rift, East-Africa - Seismic Expression and Exploration Implications." Aapg Bulletin-American Association of Petroleum Geologists 79(11): 1679-1697.

Scholz, C. A., A. S. Cohen, et al. (2011). "Southern hemisphere tropical climate over the past 145ka: Results of the Lake Malawi. Scientific Drilling Project, East Africa Preface." Palaeogeography Palaeoclimatology Palaeoecology 303(1-4): 1-2.

Scholz, C. A., T. C. Johnson, et al. (2007). "East African megadroughts between 135 and 75 thousand years ago and bearing on early-modern human origins." Proceedings of the National Academy of Sciences of the United States of America 104(42): 16416-16421.

Snyder, N. P., K. X. Whipple, et al. (2002). "Interactions between onshore bedrock-channel incision and nearshore wave-base erosion forced by eustasy and tectonics." Basin Research 14(2): 105-127.

Stone, J. R., K. S. Westover, et al. (2011). "Late Pleistocene paleohydrography and diatom paleoecology of the central basin of Lake Malawi, Africa." Palaeogeography Palaeoclimatology Palaeoecology 303(1-4): 51-70.

Walsh, J. J., A. Nicol, et al. (2002). "An alternative model for the growth of faults." Journal of Structural Geology 24(11): 1669-1675.

Whipple, K. X. (2004). "Bedrock rivers and the geomorphology of active orogens." Annual Review of Earth and Planetary Sciences 32: 151-185.

Whipple, K. X. and G. E. Tucker (1999). "Dynamics of the stream-power river incision model: Implications for height limits of mountain ranges, landscape response timescales, and research needs." Journal of Geophysical Research-Solid Earth 104(B8): 17661-17674.

Wolman, M. G. (1955). The natural channel of Brandywine Creek, Pennsylvania. Washington,, U. S. Govt. Print. Off.

Woltering, M., T. C. Johnson, et al. (2011). "Late Pleistocene temperature history of Southeast Africa: A TEX86 temperature record from Lake Malawi." Palaeogeography Palaeoclimatology Palaeoecology 303(1-4): 93-102.